The bacterial chromatin protein HupA can remodel DNA and associates with the nucleoid in *Clostridium difficile*

Ana M. Oliveira Paiva[1,3], Annemieke H. Friggen[1,3], Liang Qin[2,3], Roxanne Douwes[1], Remus T. Dame[2,3], Wiep Klaas Smits[1,3]*

1) Department of Medical Microbiology, Section Experimental Bacteriology, Leiden University Medical Center, Leiden, The Netherlands
2) Faculty of Science, Leiden Institute of Chemistry, Leiden University, Leiden, Netherlands
3) Center for Microbial Cell Biology, Leiden, The Netherlands

* Corresponding author: Department of Medical Microbiology, Section Experimental Bacteriology, Postzone E4-P, Leiden University Medical Center, PO Box 9600, 2300 RC, Leiden, The Netherlands, phone +31-71-5261229, e-mail w.k.smits@lumc.nl

Keywords: HU, bacterial chromatin protein, HupA, tethered particle motion, chromosome, fluorescence microscopy, electrophoretic mobility shift assay, bending

ORCID: AMOP: 0000-0002-6122-832X; AHF: 0000-0001-5780-2053; LQ: 0000-0002-5419-8089; RD: 0000-0003-2038-0998; RTD: 0000-0001-9863-1692; WKS: 0000-0002-7409-2847

Abstract

The maintenance and organization of the chromosome plays an important role in the development and survival of bacteria. Bacterial chromatin proteins are architectural proteins that bind DNA, modulate its conformation and by doing so affect a variety of cellular processes. No bacterial chromatin proteins of *C. difficile* have been characterized to date.

Here, we investigate aspects of the *C. difficile* HupA protein, a homologue of the histone-like HU proteins of *Escherichia coli*. HupA is a 10 kDa protein that is present as a homodimer *in vitro* and self-interacts *in vivo*. HupA co-localizes with the nucleoid of *C. difficile*. It binds to the DNA without a preference for the DNA G+C content. Upon DNA binding, HupA induces a conformational change in the substrate DNA *in vitro* and leads to compaction of the chromosome *in vivo*.

The present study is the first to characterize a bacterial chromatin protein in *C. difficile* and opens the way to study the role of chromosomal organization in DNA metabolism and on other cellular processes in this organism.

Introduction

Clostridium difficile (also known as *Clostridioides difficile*)[1] is a gram-positive anaerobic bacterium that can be found in environments like soil, water, and even meat products [2, 3]. It is an opportunistic pathogen and the leading cause of antibiotic-associated diarrhea in nosocomial infections [4]. *Clostridium difficile* infection (CDI) can present symptoms that range from mild diarrhea to more severe disease, such as pseudomembranous colitis, and can even result in death [4]. Over the past two decades the incidence of CDI worldwide, in a healthcare setting as well as in the community has increased [4-6]. *C. difficile* is resistant to a broad range of antibiotics and recent studies have reported cases of decreased susceptibility of *C. difficile* to some of the available antimicrobial therapies [7, 8]. Consequently, the interest in the physiology of the bacterium has increased in order to explore new potential targets for intervention.

The maintenance and organization of the chromosome plays an important role in the development and survival of bacteria. Several proteins involved in the maintenance and organization of the chromosome have been explored as potential drug targets [9-11]. The bacterial nucleoid is a highly dynamic structure organized by factors such as the DNA supercoiling induced by the action of topoisomerases [12], macromolecular crowding [13, 14] and interactions with nucleoid-associated proteins (NAPs) [15, 16]. Bacterial NAPs have been implicated in efficiently compacting the nucleoid while supporting the regulation of specific genes for the proliferation and maintenance of the cell [16].

NAPs are present across all bacteria and several major families have been identified [16, 17]. Some of the most abundant NAPs in the bacterial cell are bacterial chromatin proteins like the HU/IHF protein family [18, 19]. *Escherichia coli* contains three HU/IHF family proteins (αHU, βHU, IHF) that have been extensively characterized [19-22]. By contrast, *Bacillus subtilis* and several other gram-positive organisms only contain one protein of the HU/IHF protein family [17, 19, 23]. In *E. coli* disruption of αHU and/or βHU function leads to a variety of growth defects or sensitivity to adverse conditions, but HU is not essential for cell

67 survival [24, 25]. However, in *B. subtilis* the HU protein HBsu is essential for cell viability,
68 likely due to the lack of functional redundancy of the HU proteins such as in *E. coli* [17, 23].

69 In solution, most HU proteins are found as homodimers or heterodimers and are able
70 to bind DNA through a flexible DNA binding domain. The crystal structure of the *E. coli* αHU-
71 βHU heterodimer suggests the formation of higher order complexes at higher protein
72 concentrations [22]. Modeling of these complexes suggest HU proteins have the ability to
73 form higher-order complexes through dimer-dimer interaction and make nucleoprotein
74 filaments [22, 26, 27]. However, the physiological relevance of these is still unclear [18, 22,
75 27].

76 The flexible nature of the DNA-binding domain in HU proteins confers the ability to
77 accommodate diverse substrates. Most proteins bind with variable affinity and without strong
78 sequence specificity to both DNA and RNA [28]. Some bacterial chromatin proteins have a
79 clear preference for AT-rich regions [29-31] or for the presence of different structures on the
80 DNA [28, 32].

81 HU proteins can modulate DNA topology in various ways. They can stabilize
82 negatively supercoiled DNA or constrain negative supercoils in the presence of
83 topoisomerase [22, 33]. HU proteins are involved in modulation of the chromosome
84 conformation and have been shown to compact DNA [16, 26, 34]. This compaction of DNA is
85 possible through the ability of HU proteins to introduce flexible hinges and/or bend the DNA
86 [16, 26, 34, 35].

87 The ability to induce conformational changes in the DNA influences a variety of
88 cellular processes due to an indirect effect on global gene expression [36-40]. In *E. coli* HU
89 proteins are differentially expressed during the cell cycle. The αHU-βHU heterodimer is
90 prevalent in stationary phase, while during exponential growth HU is predominantly present
91 as homodimers [21]. Several studies suggest an active role of HU proteins in the
92 transcription and translation of other proteins and even in DNA replication and segregation of
93 the chromosomes [41-43].

94 The diverse roles of HU proteins are underscored by their importance for metabolism
95 and virulence in bacterial pathogens. Disruption of both HU homologues (αHU and βHU) in
96 *Salmonella typhimurium*, for example, results in the down-regulation of the pathogenicity
97 island SPI2 and consequently a reduced ability to survive during macrophage invasion [44].
98 Other studies have shown the importance of HU proteins for the adaptation to stress
99 conditions, such as low pH or antibiotic treatment [45-47]. For instance, in *M. smegmatis*
100 deletion of *hupB* leads to increased sensitivity to antimicrobial compounds [46].
101 Despite the wealth of information from other organisms, no bacterial chromatin
102 protein has been characterized to date in the gram-positive enteropathogen *Clostridium*
103 *difficile*. In this study, we show that *C. difficile* HupA (CD3496) is a legitimate homologue of
104 the bacterial HU proteins. We show that HupA exists as a homodimer, binds to DNA and co-
105 localizes with the nucleoid. HupA binding induces a conformational change of the substrate
106 DNA and leads to compaction of the chromosome. This study is the first to characterize a
107 bacterial chromatin protein in *C. difficile*.
108
109 **Results and Discussion**
110
111 **C. difficile *encodes a single HU protein, HupA***
112 To identify bacterial chromatin proteins in *C. difficile*, we searched the genome
113 sequence of *C. difficile* for homologues of characterized HU proteins from other organisms.
114 Using BLASTP (https://blast.ncbi.nlm.nih.gov/), we identified a single homologue of the HU
115 proteins in the genome of the reference strain 630 [48]; GenBank: AM180355.1), encoded
116 by the *hupA* gene (CD3496)(e-value: 1e-22). This is similar to other gram-positive
117 organisms, where also a single member of this family is found [17, 19, 23] and implies an
118 essential role of this protein on the genome organization in *C. difficile*. Moreover, lack of
119 *hupA* mutants during random transposon mutagenesis of the epidemic *C. difficile* strain
120 R20291 supports that the *hupA* gene (CDR20291_3333) is essential [49].

121 Alignment of the HupA amino acid sequence with selected homologues from other
122 organisms reveals a sequence identity varying between 58% to 38% (Fig. 1a). HupA
123 displays the highest sequence identity with *Staphylococcus aureus* HU (58%). When
124 compared to the *E. coli* HU proteins, HupA has a higher sequence identity with βHU (47%)
125 than with αHU (43%).

126 The overall structure of HU proteins is conserved and has previously been described
127 through the analysis of several nucleoid-associated proteins [19, 50]. To confirm the
128 structural similarity of the *C. difficile* HupA protein to other HU proteins, we performed a
129 PHYRE2 structure prediction [51]. All top-scoring models are based on structures from the
130 HU family. The model with the highest confidence (99.9) and largest % identity (60%) is
131 based on a structure of the *S. aureus* HU protein (PDB: 4QJU). Next, we generated a
132 structural model of HupA using SWISS-MODEL [52] and *S. aureus* HU protein (Uniprot ID:
133 Q99U17)[53] as a template. As expected, the predicted structure (Fig. 1b) is a homodimer, in
134 which each monomer contains two domains as is common for HU proteins [50, 53]. The α-
135 helical dimerization domain contains a helix-turn-helix (HTH) and the DNA-binding domain
136 consists of a protruding arm composed of 3 β-sheets (Fig. 1b). In the dimer, the two β-arms
137 form a conserved pocket that can extensively interact with the DNA [53](Fig 1a).

138 Crystal structures of HU-DNA complexes have shed light on the mode of interaction
139 of HU proteins with DNA [35, 53-55]. In the co-crystal structure of *S. aureus* HU the arms
140 embrace the minor groove of the dsDNA [53]. Proline residues at the terminus of the arms
141 cause distortion of the DNA helix, by creating or stabilizing kinks [35, 53]. Further
142 electrostatic interactions between the sides of HU dimers and the phosphate backbone
143 facilitate DNA bending [56]. In *Borrelia burgdorferi* direct interactions between the DNA
144 backbone and the α-helices of the Hbb protein dimerization domain were observed [55]. The
145 overall similarity of *C. difficile* HupA to other HU family proteins (Fig. 1a) and a similar
146 predicted electrostatic surface potential (Fig. 1c) suggest a conserved mode of DNA binding
147 for *C. difficile* HupA.

148

149 ***Mutating arginine residues in the beta-arm of HupA eliminates DNA binding***

150 Based on the alignment and structural model of HupA (Fig.1) we predict that several
151 amino acid residues in *C. difficile* HupA could be involved in the interaction with DNA.
152 Specifically, the positively charged arginine residues R55, R58 and R61 on the β-arms of
153 HupA (Fig. 1a and b) were of interest. In *B. stearothermophilus* arginine 55 of BstHU
154 (residue reference to *C. difficile*) is essential for the interaction with DNA, while residues R58
155 and R61 have a minor effect [57]. In contrast, R58 and R61 play an important role in DNA
156 binding of *E. coli* βHU [58]. In *S. aureus* substitutions of the residue R58, reduced the affinity
157 of HU for DNA while R55 and R61 were crucial for proper DNA binding [53].

158 As it has been shown that disruption of a single residue may not be sufficient to
159 abolish DNA binding [32, 57, 58], we substituted the residues R55, R58 and R61 (Fig. 1b,
160 blue sticks) in *C. difficile* HupA based on the published mutations in HU from other
161 organisms [53, 57, 58]. Residue R55 was changed to glutamine (Q), a neutral residue with
162 long side chain. R58 and R61 were replaced by glutamic acid (E) and aspartic acid (D),
163 respectively, both negatively charged residues. The resulting protein is referred to as
164 $HupA^{QED}$. Evaluation of the effect of these mutations on the electrostatic surface potential of
165 the structural model of HupA reveals that compared to the wild-type protein (Fig. 1c),
166 $HupA^{QED}$ exhibits a reduced positively charged surface of the DNA binding pocket (Fig. S1),
167 which is expected to prevent the interaction with DNA.

168 To test the DNA binding of HupA and $HupA^{QED}$ we performed gel mobility shift
169 assays. *C. difficile* HupA and $HupA^{QED}$ were heterologously produced and purified as 6x
170 histidine-tagged fusion proteins ($HupA_{6xHis}$ and $HupA^{QED}{}_{6xHis;}$ see Materials and Methods).
171 We incubated increasing concentrations of protein with different [γ-^{32}P]-labelled 38 bp
172 double-stranded DNA (dsDNA) fragments with different G+C content. When $HupA_{6xHis}$ was
173 incubated with the DNA fragment a progressive reduction in mobility as a function of protein
174 concentration is evident (Fig. 2a). At 2 μM of protein, approximately 70% of DNA is present
175 as a DNA:protein complex (Fig. 2b). This clearly demonstrates that $HupA_{6xHis}$ is capable of
176 interacting with DNA.

177 Some nucleoid-associated proteins demonstrate a preference for AT-rich regions [29,
178 30, 59]. We considered that binding of HupA could show preference for low G+C content
179 DNA, since *C. difficile* has a low genomic G+C content (29.1% G+C). We tested DNA
180 binding to dsDNA with 71.1%; 52.6% and 28.9% G+C content but observed no notable
181 difference in the affinity (Fig. 2b). Our analyses do not exclude possible sequence
182 preference or differential affinity for DNA with specific structure (e.g. bent, looped, or
183 otherwise deformed)[28, 53].

184 Having established DNA binding by $HupA_{6xHis}$, we examined the effect of replacing
185 the arginine residues in the β-arm in the same assay. When $HupA^{QED}{}_{6xHis}$ was incubated with
186 all three tested DNA fragments, no shift was observed (Fig. 2a and b). This indicates that the
187 introduction of the R55Q, R58E and R61D mutations successfully abolished binding of HupA
188 to short dsDNA probes. We conclude that the arginine residues are crucial for the interaction
189 with DNA and that the DNA-binding by HupA through the protruding β-arms is consistent
190 with DNA binding by HU homologues from other organisms [35, 53, 57].

191

192 ***Disruption of DNA binding does not affect oligomerization***

193 HU proteins from various organisms have been found to form homo- or heterodimers
194 [18, 19, 22, 53]. To determine the oligomeric state of *C. difficile* HupA protein, we performed
195 size exclusion chromatography [60]. The elution profile of the purified protein was compared
196 to molecular weight standards on a Superdex 75 HR 10/30 column. Wild-type $HupA_{6xHis}$
197 protein exhibited a single clear peak with a partition coefficient (Kav) of 0.19 (Fig. 2c). These
198 values correspond to an estimated molecular weight of a 38 kDa, suggesting a multimeric
199 assembly of $HupA_{6xHis}$ (theoretical molecular weight of monomer is 11 kDa). Similar to
200 $HupA_{6xHis}$, $HupA^{QED}{}_{6xHis}$ exhibits only one peak with a Kav of 0.20 and a calculated molecular
201 weight of 37 kDa (Fig. 2c). Thus, mutation of the residues in the DNA-binding pocket of
202 HupA did not interfere with the ability of HupA to form multimers in solution.

203 The calculated molecular weight for both proteins is higher than we would expect for
204 a dimer (22 kDa), by analogy with HU proteins from other organisms. However, we cannot

205 exclude the possibility that the conformation of the proteins affects the mobility in the size
206 exclusion experiments. To better define the oligomeric state of HupA, we performed
207 glutaraldehyde crosslinking experiments. HupA monomers cross-linked with glutaraldehyde
208 were analyzed by western-blot analysis using anti-his antibodies. Upon addition of
209 glutaraldehyde (0.0006% and 0.006%) we observed an additional signal around 23 kDa (Fig.
210 2d), consistent with a HupA dimer. No higher order oligomers were observed under the
211 conditions tested. A similar picture was obtained for $HupA^{QED}_{6xHis}$ (Fig. 2d). Together, these
212 experiments support the conclusion that HupA of *C. difficile* is a dimer in solution, similar to
213 other described HU homologues, and that the ability to form dimers is independent of DNA-
214 binding activity.
215
216 ***HupA self-interacts* in vivo**
217 Above, we have shown that HupA of *C. difficile* forms dimers *in vitro.* We wanted to
218 confirm that the protein also self-interacts *in vivo*. We developed a split-luciferase system to
219 allow the assessment of protein-protein interactions in *C. difficile*. Our system is based on
220 NanoBiT (Promega)[61] and our previously published codon-optimized variant of Nanoluc,
221 $sLuc^{opt}$ [62]. The system allows one to study protein-protein interactions *in vivo* in the native
222 host, and thus present an advantage over heterologous systems. The large (LgBit) and small
223 (SmBit) subunits of this system have been optimized for stability and minimal self-
224 association by substitution of several amino acid residues [61]. When two proteins are
225 tagged with these subunits and interact, the subunits come close enough to form an active
226 luciferase enzyme that is able to generate a bright luminescent signal once substrate is
227 added. We stepwise adapted our $sLuc^{opt}$ reporter [62] by 1) removing the signal sequence
228 (resulting in an intracellular luciferase, Luc^{opt}), 2) introducing the mutations corresponding to
229 the amino acid substitutions in NanoBiT (resulting in a full length luciferase in which SmBiT
230 and LgBiT are fused, $bitLuc^{opt}$) and finally, 3) the construction of a modular vector containing
231 a polycistronic construct under the control of the anhydrotetracycline (ATc)-inducible
232 promoter P_{tet} [63] (see Supplemental Methods).

233 To assess the ability of HupA to form multimers *in vivo*, we genetically fused HupA to
234 the C-terminus of both SmBit and LgBit subunits and expressed them in *C. difficile* under the
235 control of the ATc-inducible promoter. As controls, we assessed luciferase activity in strains
236 that express full length luciferase (bitLuc^{opt}) and combinations of HupA-fusions with or
237 without the individual complementary subunit of the split luciferase (Fig. 3). Expression of the
238 positive control bitLuc^{opt} results in a 2-log increase in luminescence signal after 1 hour of
239 induction (1954024 ± 351395 LU/OD, Fig. 3). When both HupA-fusions are expressed from
240 the same operon a similar increase in the luminescence signal is detected (264646 ±
241 122518 LU/OD at T1, Fig. 3). This signal is dependent on HupA being fused to both SmBit
242 and LgBiT, as all negative controls demonstrate low levels of luminescence that do not
243 significantly change upon induction (Fig. 3).
244 Our results indicate that HupA also self-interacts *in vivo.* However, we cannot
245 exclude that the self-interaction is facilitated by other components of the cell (e.g. DNA or
246 protein interaction partners).
247
248 ***HupA overexpression leads to a condensed nucleoid***
249 To determine if inducible expression of HupA leads to condensation of the
250 chromosome in *C. difficile*, we introduced a plasmid carrying *hupA* under the ATc-inducible
251 promoter P_{tet} into strain *630Δerm* [64]. This strain (AP106) also encodes the native *hupA* and
252 induction of the plasmid-borne copy of the gene is expected to result in overproduction of
253 HupA. AP106 cells were induced in exponential growth phase and imaged 1 hour after
254 induction. In wild-type or non-induced AP106 cells nucleoids can be seen, after staining with
255 DAPI stain, with a signal spread throughout most of the cytoplasm (Fig. 4a). In some cells a
256 defined nucleoid is observed localized near the cell center (Fig. 4a). This heterogeneity in
257 nucleoid morphology is likely a reflection of the asynchronous growth.
258 When HupA expression is not induced, the average nucleoid size is 3.10 ± 0.93 μm,
259 similar to wild-type *C. difficile* 630Δ*erm* cells (3.32 ± 1.16 μm). Upon induction of HupA
260 expression a significant decrease in size of the nucleoid is observed (Fig. 4a and b, white

261 arrow). When cells are induced with 50, 100 or 200 ng/mL ATc the average nucleoid size
262 was 1.91 ± 0.80 µm; 1.90 ± 0.82 µm and 2.02 ± 0.94 µm, respectively (Fig. 4b). No
263 significant difference was detected between the strains induced with different ATc
264 concentrations (Fig. 4b).

265 In wild-type *C. difficile* 630Δ*erm* cells the average cell length is 5.14 ± 1.07 µm,
266 similar to non-induced AP106 cells (5.18 ± 1.09 µm, Fig. 4c). In the presence of increasing
267 amounts of ATc a small but significant increase of cell length is observed after 1 hour
268 induction. When cells are induced with 50, 100 or 200 ng/mL ATc the average cell length
269 was 5.79 ± 1.29 µm; 5.58 ± 1.14 µm and 6.07 ± 1.37 µm, respectively (Fig. 4c). We did not
270 observe an impairment of septum formation and localization (data not shown).

271 The decrease in the nucleoid size when HupA is overexpressed suggests that HupA
272 can compact DNA *in vivo*. This observation is reminiscent of effects of HU overexpression
273 reported for other organisms, like *B. subtilis* and *Mycobacterium tuberculosis* [10, 23].

274

275 ***HupA co-localizes with the nucleoid***

276 If HupA indeed is directly involved in condensing the nucleoid, it is expected that the
277 protein co-localizes with the DNA. To test this, we imaged HupA protein and the nucleoid in
278 live *C. difficile*. Here, we used the HaloTag protein (Promega)[65] for imaging the subcellular
279 localization of HupA. Tags that become fluorescent after covalently labeling by small
280 compounds, such as HaloTag, are proven to be useful for studies in bacteria and yeast [66-
281 68]. Different from GFP, this type of tag does not require the presence of oxygen for
282 maturation and should allow live-cell imaging in anaerobic bacteria.

283 We introduced a modular plasmid expressing HupA-HaloTag from the ATc-inducible
284 promoter P_{tet} [63] into strain 630Δ*erm* [64], yielding strain RD16. Repeated attempts to
285 create a construct that would allow us to integrate the fusion construct on the chromosome
286 of *C. difficile* using allelic exchange failed, likely due to toxicity of the *hupA* upstream region
287 in *E. coli* (cloning intermediate). For the visualization of HupA-HaloTag we used the Oregon
288 green substrate, that emits at Em_{max} 520 nm. Although autofluorescence of *C. difficile* has

289 been observed at wavelengths of 500-550 nm [69, 70] we observed limited to no green
290 signal in the absence of the HaloTag (our unpublished observations and Fig. 5a, -ATc).

291 HupA-Halotag expression was induced in RD16 cells during exponential growth
292 phase with 200 ng/mL ATc and cells were imaged after 1 hour of induction. In the absence
293 of ATc, no green fluorescent signal is visible, and the nucleoid (stained with DAPI) appears
294 extended (Fig. 5a). Upon HupA-HaloTag overexpression, the nucleoids are more defined
295 and appear bilobed (Fig. 5a and b), similar to previous observations (Fig. 4a). The Oregon
296 Green signal co-localizes with the nucleoid, located in the center of the cells, with a bilobed
297 profile that mirrors the profile of the DAPI stain (Fig. 5a and b). This co-localization is
298 observed for individual cells at different stages of the cell cycle and is independent of the
299 number of nucleoids present (data not shown). The localization pattern of the *C. difficile*
300 HupA resembles that of HU proteins described in other organisms [23, 71, 72] (Fig 5a).
301 Expression levels of HupA-Halotag were confirmed by SDS-PAGE in-gel fluorescence of
302 whole cell extracts, after incubation with Oregon Green (Fig. 5c).

303 ATc-induced RD16 cells exhibit a heterogeneous Oregon Green fluorescent signal.
304 This has previously been observed with other fluorescent reporters in *C. difficile* [68-70, 73]
305 and can likely be explained by both heterogeneous expression from inducible systems [74]
306 and different stages of the cell cycle. For instance, the localization of cell division proteins,
307 such as MldA or FtsZ is dependent on septum formation and thus dependent on cells
308 undergoing cell division [69, 73].

309 We found that $HupA^{QED}_{6xHis}$ does not bind dsDNA in the electrophoretic mobility shift
310 assay (Fig. 2b). We introduced the triple substitution in the HupA-HaloTag expression
311 plasmid to determine its effect on localization of the protein in *C. difficile.* We found that the
312 $HupA^{QED}$-HaloTag protein was broadly distributed throughout the cell and that - different from
313 ATc-induced RD16 cells (HupA-Halotag) - no compaction of the nucleoid occurred (Fig. 5a).
314 The lack of compaction is not due to lower expression levels of $HupA^{QED}$-Halotag compared
315 to HupA-HaloTag, as induced levels of both proteins are similar (Fig. 5c).

316 The nucleoid morphology upon expression of HupA^{QED}-HaloTag is similar to that
317 observed in wild type 630Δ*erm* cells (Fig. 4a), suggesting that HupA^{QED} does not influence
318 the activity of the native HupA *in vivo*. Though the mutated residues did not affect
319 oligomerization (Fig. 2c and d) we considered the possibility that HupA^{QED} is unable to form
320 heterodimers with native HupA. To evaluate whether HupA^{QED} and HupA can interact, we
321 performed glutaraldehyde crosslinking and an *in vivo* complementation assay (Fig. S2). To
322 allow for discrimination between momoners of wild type and mutant HupA in the crosslinking
323 assay, we purified the HupA-HaloTag from *C. difficile* and incubated this protein with
324 heterologously produced and purified HupA$_{6xHis}$ or HupA$^{QED}{}_{6xhis}$. Upon crosslinking bands
325 corresponding to dimers of the his-tagged (22 kDa) and the HaloTagged protein (96 kDa)
326 are detectable (Fig. S2a), confirming our previous results (Fig. 2d). We also detect a signal
327 corresponding to the molecular weight of a heterodimer with both HupA$_{6xhis}$ and HupA$^{QED}{}_{6xhis}$
328 (56 kDa), suggesting that wild type and mutant protein can form heterodimers *in vitro* (Fig
329 S2a). To analyze the *in vivo* behavior of these proteins, HupA^{QED} was expressed fused to
330 SmBit and HupA to LgBit in the split luciferase complementation assay. In line with the
331 crosslinking experiment, we observe luciferase reporter activity that is similar to that
332 observed for AP122 (HupA-SmBiT/HupA-LgBiT). Thus, mutation of the arginine residues
333 does not abolish the interaction with HupA *in vivo*. Nevertheless, it is conceivable that wild
334 type homodimers are preferentially formed *in vivo* despite expression of HupA^{QED}: the lack of
335 DNA binding by HupA^{QED} could result in an effectively lower local concentration in the
336 nucleoid than for wild type HupA.

337 Together, these results indicate that HupA co-localizes with the nucleoid, and that
338 nucleoid compaction upon HupA overexpression is possibly dependent on its DNA-binding
339 activity. We cannot exclude that the nucleoid compaction observed is an indirect result of
340 HupA overexpression by influencing possible interaction with RNA and/or other proteins, or
341 by altering transcription/translation [40, 75].

342

343 ***HupA compacts DNA* in vitro**

344 To substantiate that the decrease in nucleoid size is directly attributable to the action
345 of HupA, we sought to demonstrate a remodeling effect of HupA on DNA *in vitro*. We
346 performed a ligase-mediated DNA cyclization assay. Previous work has established that a
347 length smaller than 150 bp greatly reduces the possibility of the extremities of dsDNA
348 fragments to meet. This makes the probability to ligate into closed rings less [76]. However,
349 in the presence of DNA bending proteins exonuclease III (ExoIII)-resistant (thus closed)
350 rings can be obtained [56, 76].

351 We tested the ability of $HupA_{6xHis}$ to stimulate cyclization of a [γ-^{32}P]-labeled 123-bp
352 DNA fragment (Fig. 6a). The addition of T4 DNA-ligase alone results in multiple species,
353 corresponding to ExoIII-sensitive linear multimers (Fig. 6a, lane 2 and 3). In the presence of
354 $HupA_{6xHis}$, however, an ExoIII-resistant band is visible (Fig. 6a, lanes 4 to 6). In the absence
355 of ExoIII, the linear dimer is still clearly visible in the HupA-containing samples (Fig. 6a, last
356 lane). We conclude that *C. difficile* HupA is able to bend the DNA, or otherwise stimulate
357 cyclization by increasing flexibility and reducing the distance between the DNA fragment
358 extremities, allowing the ring closure in the presence of ligase.

359 To more directly demonstrate remodeling of DNA by HupA, we performed tethered
360 particle motion (TPM) experiments. TPM is a single molecule technique that provides a
361 readout of the length and flexibility of a DNA tether (Supplemental Fig. S3)[77]. The binding
362 of proteins to DNA alters its conformation, resulting in a change in RMS (Root Mean
363 Square). If a protein bends DNA, makes DNA more flexible or more compact, the RMS is
364 reduced compared to that of bare DNA, as represented in Supplemental Fig. S3 [77]. If a
365 protein stiffens DNA, the RMS is expected to be larger than that of bare DNA [78].

366 We performed TPM experiments according to established methods [78] to determine
367 the effects of HupA on DNA conformation at protein concentrations from 0 – 1600 nM (Fig.
368 6b). For this assay a non-tagged HupA was purified from *C. difficile* cells overexpressing
369 HupA and compared to $HupA_{6xHis}$ to assess potential subtle effects of the 6xhistidine-tag on
370 the protein functionality. The experiments show that binding of both native HupA and
371 $HupA_{6xHis}$ to DNA reduces the RMS (Fig. 6b). The RMS of bare DNA is 148 ± 1.9 nm. In the

372 presence of HupA at different concentrations (100, 200, 400 nM) the RMS decreases (113 ±
373 0.1 nm; 103 ± 0.7 nm and 97 ± 1.5 nm respectively). Even at higher concentrations of HupA
374 (800, 1600 nM) the RMS is 97-100 nm. $HupA^{QED}_{6xHis}$ did not affect RMS even at high protein
375 concentrations (Fig. 6b). The strongly reduced RMS of DNA bound by non-tagged HupA at
376 1600 nM suggests a more compacted conformation of DNA compared to that of bare DNA.
377 The curves are overall highly similar for HupA and $HupA_{6xHis}$ proteins; the small difference in
378 the observed effects is attributed to interference of the tag and/or protein stability. The
379 results obtained with the $HupA^{QED}_{6xhis}$ protein indicate that DNA binding by HupA is crucial
380 for compaction, as expected. We also tested the effect of the addition of a two-fold molar
381 excess of $HupA^{QED}_{6xhis}$ on DNA compaction in the presence of 400 nM HupA in a TPM
382 experiment, but observed no significant difference (data not shown). This indicates that
383 under these conditions $HupA^{QED}_{6xhis}$ does not remove DNA-bound HupA or affects its ability
384 to remodel the DNA.

385 The effects of *C. difficile* HupA on DNA conformation observed by TPM indicate
386 structural properties similar to those of *E. coli* HU, which was shown to compact DNA by
387 bending at low protein coverage [26, 79, 80]. However, in contrast to *E. coli* [26], there is no
388 clear stiffening of the DNA tether at high concentrations of protein in our assay, suggesting
389 that there is lower or reduced dimer-dimer interaction in our experimental condition. Bending
390 of DNA by HU proteins has also been shown for other organisms. Interestingly, in *B.*
391 *burgdorferi* [55] and *Anabaena* [35] it was shown that bending is influenced by interaction of
392 the DNA with a positively charged lateral surface, although the main interaction region with
393 the DNA is through the β-arms. *C. difficile* HupA demonstrates an electrostatic surface
394 potential compatible with such a mechanism (Fig 1C). It will be of interest to determine if and
395 which residues in this region contribute to the bending of the DNA.

396

397 **Overexpression of HupA decreases cell viability**

398 The condensation of the nucleoid and the slight increase of cell length during the
399 time course of our microscopy experiments (Fig. 4b and c) could indicate that

400 overexpression of HupA interferes with crucial cellular processes such as DNA replication.
401 We therefore determined the long term effect of HupA overexpression on cell viability in a
402 spot-assay (Fig. 7). In the absence of inducer, *C. difficile* strains harboring inducible *hupA*
403 genes grow as well as the vector control (AP34), with colonies visible at the 10^{-5} dilution.
404 However, when induced with 200 ng/ml ATc viability is markedly reduced for strains
405 overexpressing HupA (5-log; AP106), HupA-HaloTag (4-log; RD16) and $HupA^{QED}$-HaloTag
406 (1 to 2-log; AF239) compared to the vector control. These effects are not due to a direct
407 inhibitory effect of ATc alone, as the viability of AP34 is similar under both conditions.

408 We consistently observed a 1-log difference in cell viability between cells expressing
409 HupA versus HupA-HaloTag (Fig. 7). This difference could be the result of slight interference
410 of the HaloTag with HupA function, as also observed for the 6xhistagged protein in the TPM
411 experiments (Fig. 6b). Considering that $HupA^{QED}$ does not appear to bind or compact DNA
412 (Figs. 2, 5 and 6), the moderate reduction in cell viability compared to the vector control
413 could be due to a dominant negative effect: the formation of heterodimers, consistent with
414 our analysis (Fig. S2), could prevent a fraction of wild type HupA performing its essential
415 function.

416 Overall, these results are consistent with an important role of HupA in chromosome
417 dynamics.

418

419 ***Conclusions***

420 In this work, we present the first characterization of a bacterial chromatin protein in *C.*
421 *difficile*. HupA is a member of the HU family of proteins and is capable of binding DNA and
422 does so without an obvious difference in affinity as a result of the G+C content. DNA binding
423 is dependent on the residues R55, R58 and R61 that are located in the predicted β-arm of
424 the protein. These observations in combination with the predicted structure suggest a
425 conserved mode of DNA binding, although the role of other regions of the protein in DNA

426 binding is still poorly understood. HupA is present as a dimer in solution and disruption of the
427 residues of the DNA binding domain did not affect the oligomeric state of HupA.

428 In *C. difficile* we co-localized HupA with the nucleoid and demonstrated that
429 overexpression of HupA leads to nucleoid compaction and impairs *C. difficile* viability. In line
430 with these observations, HupA stimulates the cyclization of a short dsDNA fragment and
431 compacts DNA *in vitro*.

432 We also developed a new complementation assay for the detection of protein-protein
433 interactions in *C. difficile,* complementing the available tools for this organism, and confirmed
434 that HupA self-interacts *in vivo*. Additionally, to our knowledge, our study is the first to
435 describe the use of the fluorescent tag HaloTag for imaging the subcellular localization of
436 proteins in live *C. difficile* cells.

437 In sum, HupA of *C. difficile* is an essential bacterial chromatin protein required for
438 nucleoid (re)modelling. HupA binding induces bending or increases the flexibility of the DNA,
439 resulting in compaction. The precise role of HupA in chromosome dynamics *in vivo* remains
440 to be determined. In *E. coli* conformational changes resulting from HU proteins enhance
441 contacts between distant sequences in the chromosome [81]. In *Caulobacter*, HU proteins
442 promote contacts between sequences in more close proximity [82]. These differences
443 demonstrate that HU proteins despite high sequence similarity may act differently as a
444 function of *in vivo* context and that further research into the role of HupA in *C. difficile*
445 physiology is needed.

446

447

448 **Methods**

449

450 *Sequence Alignments and Structural Modelling*

451 Multiple sequence alignment of amino acid sequences was performed with Clustal
452 Omega [83]. The sequences of HU proteins identified in *C. difficile* 630Δ*erm* (Q180Z4), *E.*
453 *coli* (P0ACF0 and P0ACF4), *Bacillus subtilis* (A3F3E2), *Geobacillus stearothermophilus*
454 (P0A3H0), *Bacillus anthracis* (Q81WV7), *Staphylococcus aureus* (Q99U17), *Salmonella*
455 *typhimurium* (P0A1R8), *Streptococcus pneumoniae* (AAK75224), *S. mutans* (Q9XB21), *M.*
456 *tuberculosis* (P9WMK7), *Thermotoga maritima* (P36206) and *Anabaena sp.* (P05514), were
457 selected for alignment. Amino acid sequences were retrieved from the Uniprot database.

458 Homology modelling was performed using PHYRE2
459 (http://www.sbg.bio.ic.ac.uk/phyre2, [51] and SWISS-MODEL [52] using default settings. For
460 SWISS-MODEL, PDB 4QJN was used as a template. Selection of the template was based
461 on PHYRE2 results, sequence identity (59,55%) and best QSQE (0,80) and GMQE (0,81).
462 Graphical representations and mutation analysis were performed with the PyMOL Molecular
463 Graphics System, Version 1.76.6. Schrödinger, LLC. For electrostatics calculations APBS
464 (Adaptive Poisson-Boltzmann Solver) and PDB2PQR software packages were used [84].
465 Default settings were used.

466

467 *Strains and growth conditions*

468 *E. coli* strains were cultured in Luria Bertani broth (LB, Affymetrix) supplemented with
469 chloramphenicol at 15 µg/mL or 50 µg/mL kanamycin when appropriate, grown aerobically at
470 37°C. Plasmids (Table 1) were maintained in *E. coli* strain DH5α. Plasmids were
471 transformed using standard procedures [85]. *E. coli* strain Rosetta (DE3) (Novagen) was
472 used for protein expression and *E. coli* CA434 for plasmid conjugation [86] with *C. difficile*
473 strain 630Δ*erm* [64, 87].

474 *C. difficile* strains were cultured in Brain Heart Infusion broth (BHI, Oxoid), with 0,5 %
475 w/v yeast extract (Sigma-Aldrich), supplemented with 15 µg/mL thiamphenicol and

476 *Clostridium difficile* Selective Supplement (CDSS; Oxoid) when necessary. *C. difficile* strains
477 were grown anaerobically in a Don Whitley VA-1000 workstation or a Baker Ruskinn
478 Concept 1000 workstation with an atmosphere of 10% H_2, 10% CO_2 and 80% N_2.
479 The growth was followed by optical density reading at 600 nm. All the *C. difficile*
480 strains are described in Table 2.
481
482 *Construction of the E. coli expression vectors*
483 All oligonucleotides and plasmids from this study are listed in Tables 1 and 3.
484 To construct an expression vector for $HupA_{6xHis}$, the *hupA* gene (CD3496 from *C.*
485 *difficile* 630 GenBank accession no. NC_009089.1) was amplified by PCR from *C. difficile*
486 630Δ*erm* genomic DNA using primers oAF57 and oAF58 (Table 3). The product was
487 inserted into the *Nco*I-*Xho*I digested pET28b vector (Table 1) placing it under control of the
488 T7 promoter, yielding plasmid pAF226.
489 To generate the HupA triple mutant ($HupA^{QED}_{6xHis}$) site-directed mutagenesis was
490 used according to the QuikChange protocol (Stratagene). Initially the arginine at position 55
491 and at position 58 were simultaneously substituted for glutamine (R55Q) and glutamic acid
492 (R58E) respectively, using primers oAF73/oAF74 (Table 3), resulting in pAF232 (Table 1).
493 The arginine at position 61 was subsequently substituted for aspartic acid (R61D) using
494 primer pair oAF75/oAF76 (Table 3) and pAF232 as a template, yielding pAF234 (Table 1).
495 All the constructs were confirmed by Sanger sequencing.
496
497 *Construction of the C. difficile expression vectors*
498 To overexpress non-tagged HupA the *hupA* gene was amplified by PCR from *C.*
499 *difficile 630Δerm* genomic DNA using primers oWKS-1519 and oAP47 (Table 3) and cloned
500 into SacI-BamHI digested pRPF185 vector [63], placing it under control of the ATc-inducible
501 promoter P_{tet}, yielding vector pAP103 (Table 1).

502 For microscopy experiments HaloTagged protein (Promega) was used. The *halotag*
503 gene was amplified from vector pH6HTC (Promega, GenBank Accession no. JN874647)
504 with primers oWKS-1511/oWKS-1512 and inserted into pCR2.1-TOPO according to the
505 instructions of the manufacturer (ThermoFisher), yielding vector pWKS1746 (Table 1). This
506 primer combination also introduces a 6xHis-tag at the C-terminus of the HaloTag. The *hupA*
507 gene was amplified with primers oWKS-1519/oWKS-1520 (Table 3) and inserted into vector
508 pCR2.1-TOPO according to the instructions of the manufacturer (ThermoFisher), generating
509 vector pWKS1744 (Table 1). The primers introduces the *cwp2* ribosomal binding site
510 upstream and a short DNA sequence encoding a GS-linker downstream (SGSGSGS) of the
511 *hupA* open reading frame. To generate the expression construct for HupA-Halotag the open
512 reading frame encoding the $HaloTag_{6xHis}$ protein was amplified from pWKS1746 using
513 primers oRD5/oWKS-1512 (Table 3). The *hupA* gene was amplified from pWKS1744 with
514 primers oWKS-1519/oWKS-1520 (Table 3). Gene fusions were made by overlapping PCR
515 using the PCR amplified fragments encoding HupA and Halotag proteins as templates with
516 primers oWKS-1519 and oWKS-1512 (Table 3). The fragment was cloned into SacI-BamHI
517 digested pRPF185 [63], placing it under control of the ATc inducible promoter P_{tet}, yielding
518 vector pRD4 (Table 1).
519 To generate the HupA triple mutant fused to the Halotag ($HupA^{QED}$-Halotag) site-
520 directed mutagenesis was used, according to the QuikChange protocol (Stratagene). The
521 arginines at position 55 and at position 58 were substituted to glutamine (R55Q) and
522 glutamic acid (R58E), using primers oAF73/oAF74 (Table 3) and pRD4 as template,
523 resulting in pAF235 (Table 1). The arginine at position 61 was subsequently substituted to
524 aspartic acid (R61D), using pAF235 as template and primers oAF75/oAF76 (Table 3),
525 yielding pAF237 (Table 1). All the constructs were confirmed by Sanger sequencing.
526
527
528 *Construction of the bitLuc^{opt} expression vectors*

529 The bitLuc^{opt} complementation assay for *C. difficile* described in this study is based
530 on NanoBiT (Promega) [61] and the codon optimized sequence of sLuc^{opt} [62]. Details of its
531 construction can be found in Supplemental Material.

532 Gene synthesis was performed by Integrated DNA Technologies, Inc. (IDT).
533 Fragments were amplified by PCR from synthesized dsDNA, assembled by Gibson
534 assembly [88] and cloned into *Sac*I/*BamH*I digested pRPF185 [63], placing them under
535 control of the ATc-inducible promoter P_{tet}. As controls a non-secreted luciferase (Luc^{opt};
536 pAF254) and a luciferase with the NanoBiT aminoacid substitutions (Promega)[61](bitLuc^{opt};
537 pAF259) were constructed. We also constructed vectors expressing only the SmBiT and
538 LgBiT domains, alone (pAF260 and pAF255) or in combination (pAF262), as controls.

539 To assay for a possible interaction between HupA monomers, vectors were
540 constructed that encode HupA-SmBiT/HupA-LgBiT (pAP118), HupA^{QED}-SmBiT/HupA-LgBiT
541 (pAP210), HupA-SmBiT/LgBiT (pAF256), SmBiT/HupA-LgBiT (pAF257). DNA sequences of
542 the cloned DNA fragments in all recombinant plasmids were verified by Sanger sequencing.

543 Note that all our constructs use the HupA start codon (GTG) rather than ATG; a
544 minimal set of vectors necessary to perform the *C. difficile* complementation assay (pAP118,
545 pAF256, pAF257 and pAF258) is available from Addgene (105494-105497) for the *C.*
546 *difficile* research community.

547

548 *Overproduction and purification of* HupA$^{(QED)}{}_{6xhis}$ and HupA-HaloTag

549 Overexpression of HupA$_{6xHis}$ and HupA$^{QED}{}_{6xHis}$ was carried out in *E. coli* Rosetta
550 (DE3) strains (Novagen) harbouring the *E. coli* expression plasmids pAF226 and pAF234,
551 respectively. Cells were grown in LB and induced with 1mM isopropyl-β-D-1-
552 thiogalactopyranoside (IPTG) at an optical density (OD_{600}) of 0,6 for 3 hours. The cells were
553 collected by centrifugation at 4°C and stored at -80°C.

554 Overexpression of HupA-HaloTag (which also includes a 6xhistag) was carried out in
555 *C. difficile* strains RD16. Cells were grown until OD_{600} 0.4-0.5 and induced with 200 ng/mL
556 ATc for 1 hour. Cells were collected by centrifugation at 4°C and stored at -80°C.

557 Pellets were suspended in lysis buffer (50 mM NaH_2PO_4 (pH 8.0), 300 mM NaCl, 10
558 mM imidazole, 5 mM β mercaptoethanol, 0.1% NP40 and Complete protease inhibitor
559 cocktail (CPIC, Roche Applied Science). Cells were lysed by the addition of 1 mg/ml
560 lysozyme and sonication. The crude lysate was clarified by centrifugation at 13000 g at 4°C
561 for 20 min. The supernatant containing recombinant proteins was collected and purification
562 was performed with TALON Superflow resin (GE Healthcare) according to the
563 manufacturer's instructions. Proteins were stored at -80°C in 50 mM NaH_2PO_4 (pH 8.0), 300
564 mM NaCl and 12% glycerol.
565
566 *Overproduction and purification of non-tagged HupA*
567 Overexpression of HupA was carried out in *C. difficile* strain AP106 that carries the
568 plasmid encoding HupA under the ATc-inducible promoter P_{tet}. Cells were grown until OD_{600}
569 0.4-0.5 and induced with 200 ng/mL ATc for 3 hours. Cells were collected by centrifugation
570 at 4°C.
571 Pellets were resuspended in HB buffer (25 mM Tris (pH 8.0), 0.1 mM EDTA, 5 mM β
572 mercaptoethanol, 10% glycerol and CPIC). Cells were lysed by French Press and
573 phenylmethylsulfonyl fluoride was added to 0.1 mM. Separation of the soluble fraction was
574 performed by centrifugation at 13000g at 4°C for 20 min. Purification of the protein from the
575 soluble fraction was done on a 1 mL HiTrap SP (GE Healthcare) according to manufacturer
576 instructions. The protein was collected in HB buffer supplemented with 300 mM NaCl.
577 Fractions containing the HupA protein were pooled together and applied to a 1 mL Heparin
578 Column (GE Healthcare) according to manufacturer's instructions. Column washes were
579 performed with a 500 mM – 800 mM NaCl gradient in HB buffer. Proteins were eluted in HB
580 buffer supplemented with 1 M NaCl and stored in 10% glycerol at -80°C.
581
582 *DNA labelling and electrophoretic mobility shift Assay (EMSA)*
583 For the gel shift assays double stranded oligonucleotides with different GC contents
584 were used. Oligonucleotides oAF61/oAF62 have a 71,1% G+C-content, oAF63/oAF64 have

585 a 52,6% G+C-content and oAF65/oAF66 have a 28,9% G+C-content. The oligonucleotides
586 were labelled with [ɣ-^{32}P]ATP and T4 polynucleotide kinase (PNK) (Invitrogen) according to
587 the PNK-manufacturer's instructions. The fragments were purified with a Biospin P-30 Tris
588 column (BioRad). Oligonucleotides with same G+C content were annealed by incubating
589 them at 95˚C for 10 min, followed by ramping to room temperature.

590 Gel shift assays were performed with increasing concentrations (0,25 -2 μM) of
591 $HupA_{6xHis}$ or $HupA^{QED}_{6xHis}$ in a buffer containing 20 mM Tris pH 8.0; 50 mM NaCl; 12 mM
592 $MgCl_2$; 2.5 mM ATP; 2 mM DTT; 10% glycerol and 2.4 nM [ɣ-^{32}P]ATP-labelled
593 oligonucleotides. Proteins were incubated with the oligonucleotide substrate for 20 min at
594 room temperature prior to separation. Reactions were analyzed in 8% native polyacrylamide
595 gels in cold 0,5X TBE buffer supplemented with 10 mM $MgCl_2$. After electrophoresis gels
596 were dried under vacuum and protein-DNA complexes were visualized by phosphorimaging
597 (Typhoon 9410 scanner; GE Healthcare). Analysis was performed with Quantity-One
598 software (BioRad).

599

600 *Size-exclusion chromatography*

601 Size-exclusion experiments were performed on an Äkta pure 25L1 instrument (GE
602 Healthcare). 200 μL of $HupA_{6xHis}$ and $HupA^{QED}_{6xHis}$ was applied at a concentration of ~100
603 μM, to a Superdex 75 HR 10/30 column (GE Healthcare), in buffer containing 50 mM
604 NaH_2PO_4 (pH 8.0), 300 mM NaCl and 12% glycerol. UV detection was done at 280 nm.
605 Lower concentrations of HupA were not possible to analyses due to the lack of signal. HupA
606 protein only contains 3 aromatic residues, and lacks His, Trp, Tyr or Cys to allow detection
607 by absorbance at 280 nm. The column was calibrated with a mixture of proteins of known
608 molecular weights (Mw): Conalbumin (75 kDa), Ovalbumin (44 kDa), Carbonic anhydrase
609 (29 kDa), Ribonuclease A (13,7 kDa), and Aprotinin (6,5 kDa). Molecular weight of the HupA
610 proteins was estimated according to the equation MW=10(Kav-b)/m where m and b
611 correspond to the slope and the linear coefficient of the plot of the logarithm of the MW as a
612 function of the Kav. The Kav is given by the equation $Kav=(V_e-V_0)/(V_t-V_0)$ [89], where V_e is

613 the elution volume for a given concentration of protein, V_0 is the void volume (corresponding
614 to the elution volume of thyroglobulin), and V_t is the total column volume (estimated from the
615 elution volume of a 4% acetone solution).
616
617 *Glutaraldehyde cross-linking Assay*
618 100 ng HupA protein was incubated with different concentrations of glutaraldehyde (0
619 0,006%) for 30 min at room temperature. Reactions were quenched with 10 mM Tris. The
620 samples were loaded on a 6.5% SDS-PAGE gel and analysed by western-blotting. The
621 membrane was probed with a mouse anti-His antibody (Thermo Fisher) 1:3000 in phosphate
622 buffered saline (PBS; 137 mM NaCl, 2.7 mM KCl, 4.3 mM Na_2HPO_4, 1.47 mM KH_2PO_4) with
623 0.05% Tween-20 and 5% w/v Milk (Campina), a secondary anti-mouse HRP antibody 1:3000
624 and Pierce ECL2 Western blotting substrate (Thermo Scientific). A Typhoon 9410 scanner
625 (GE Healthcare) was used to record the chemiluminescent signal.
626
627 *Split luciferase (bitLuc^{opt}) Assay*
628 For the *C. difficile* complementation assay, cells were grown until OD_{600} 0.3-0.4 and
629 induced with 200 ng/mL anhydrotetracline for 60 min. To measure luciferase activity 20 µL
630 NanoGlo Luciferase (Promega N1110) was added to 100 µL of culture sample.
631 Measurements were performed in triplicate in a 96-well white F-bottom plate according to
632 manufacturer's instructions. Luciferase activity was determined using a GloMax instrument
633 (Promega) for 0.1 s. Data was normalized to culture optical density measured at 600 nm
634 (OD_{600}). Statistical analysis was performed with Prism 7 (GraphPad, Inc, La Jolla, CA) by
635 two-way ANOVA.
636
637 *Ligase-mediated cyclization assay*
638 A 119 bp DNA fragment was amplified by PCR amplification with primers
639 oAF81/oAF82, using pRPF185 plasmid as a template. The PCR fragment was digested with
640 *EcoR*I and 5'end labelled with [$\gamma 3^2$P] ATP using T4 polynucloetide kinase (Invitrogen)

641 according to the manufacturer's instructions. Free ATP was removed with a Biospin P-30
642 Tris column (BioRad).

643 The labelled DNA fragment (~0.5 nM) waspAF235 incubated with different
644 concentrations of HupA for 30 min on 30°C in 50 mM Tris-HCl, pH 7.8, 10 mM $MgCl_2$, 10
645 mM DTT, and 0.5 mM ATP in a total volume of 10 µl. 1 Unit of T4 ligase was added and
646 incubated for 1 h at 30°C followed by inactivation for 15 minutes at 65°C. When appropriate,
647 samples were treated with 100 U of Exonuclease III (Promega) at 37°C for 30 minutes.
648 Enzyme inactivation was performed by incubating the samples for 15 minutes at 65°C.
649 Before electrophoresis the samples were digested with 2 µg proteinase K and 0.2% SDS at
650 37°C for 30 minutes. Samples were applied to a pre-run 7% polyacrylamide gel in 0.5X TBE
651 buffer with 2% glycerol and run at 100V for 85 min. After electrophoresis the gel was
652 vacuum-dried and analysed by phosphor imaging. Analysis was performed with Quantity-
653 One software (BioRad).

654

655 *Fluorescence microscopy*

656 The sample preparation for fluorescence microscopy was carried out under
657 anaerobic conditions. *C. difficile* strains were cultured in BHI/YE, and when appropriate
658 induced with different ATc concentrations (50, 100 and 200 ng/mL) for 1 hour at an OD_{600} of
659 0.3-0.4. When required, cells where incubated with 150 nM Oregon Green substrate for
660 HaloTag (Promega) for 30 min. 1 mL culture was collected and washed with pre-reduced
661 PBS. Cells were incubated with 1 µM DAPI (Roth) when necessary. Cells were spotted on
662 1.5% agarose patches with 1 µL of ProLong Gold antifading mountant (Invitrogen). Slides
663 were sealed with nail polish.

664 Samples were imaged with a Leica DM6000 DM6B fluorescence microscope (Leica)
665 equipped with DFC9000 GT sCMOS camera using a HC PLAN APO 100x/1.4 OIL PH3
666 objective, using the LAS X software. The filter set for imaging DAPI is the DAPI ET filter (n.
667 11504203, Leica), with excitation filter 350/50 (band pass), long pass dichroic mirror 400 and
668 emission filter 460/50 (band pass). For imaging of Oregon Green the filter L5 ET was used

669 (n. 11504166, Leica), with excitation filter 480/40, dichroic mirror 505 and emission filter
670 527/30.
671 Data was analyzed with MicrobeJ package version 5.12d [90] with ImageJ 1.52d
672 software [91]. Recognition of cells was limited to 2 - 16 µm length. For the nucleoid and
673 Halotag detection the nucleoid feature was used for the nucleoid length and fluorescent
674 analysis. Cells with more than 2 identified nucleoids and defective detection were excluded
675 from analysis. Statistical analysis was performed with MicrobeJ package version 5.12d [90].
676
677 *In-gel fluorescence*
678 *C. difficile* strains were cultured in BHI/YE, and when appropriate induced at an
679 OD_{600} of 0.3-0.4 with 200 ng/mL ATc concentrations for up to 3 hours. Samples were
680 collected and centrifuged at 4°C. Pellets were resuspended in PBS and lysed by French
681 Press. Samples were incubated with 150 nM Oregon Green substrate for HaloTag
682 (Promega) for 30 minutes at 37°C. Loading buffer (250 mM Tris-Cl pH 6.8, 10 % SDS, 10%
683 β-mercaptoethanol, 50% glycerol, 0.1% bromophenol blue) was added to the samples
684 without boiling and samples were run on 12% SDS-PAGE gels. Gels were imaged with
685 Uvitec Alliance Q9 Advanced machine (Uvitec) with F-535 filter (460 nm).
686
687 *Spot assay*
688 Cells were grown until OD_{600} of 1.0 in BHI/YE. The cultures were serially diluted (10^0
689 to 10^{-5}) and 2 µL from each dilution were spotted on BHI/YE supplemented with CDSS,
690 thiamphenicol and 200 ng/mL ATc when appropriate. Plates were imaged after 24 hours
691 incubation at 37ºC.
692
693 *Tethered Particle Motion measurements*
694 A dsDNA fragment of 685bp with 32% G+C content (sso685) was used for Tethered
695 Particle Motion experiments. This substrate was generated by PCR using the forward biotin-
696 labelled primer Sso10a-2Nde and the reverse digoxygenin (DIG) labelled primer Sso10a-

697 2Bam685 from pRD118 as previously described [92]. The PCR product was purified using
698 the GenElute PCR Clean-up kit (Sigma-Aldrich).

699 Tethered Particle Motion (TPM) measurements were done as described previously
700 [77, 78] with minor modifications. In short, anti-digoxygenin (20 µg/mL) was flushed into the
701 flow cell and incubated for 10 minutes to allow the anti-digoxygenin to attach to the glass
702 surface. To block unspecific binding to the glass surface, the flow cell was incubated with
703 BSA and BGB (Blotting grade Blocker) in buffer A (10 mM Tris (pH 7.5), 150 mM NaCl, 1
704 mM EDTA, 1 mM DTT, 3% glycerol, and 100 µg/mL acetylated BSA, 0.4% BGB) for 10
705 minutes. To tether DNA to the surface, DNA (labeled with Biotin and DIG) diluted in buffer B
706 (10 mM Tris (pH 7.5), 150 mM NaCl, 1 mM EDTA, 1 mM DTT, 3% glycerol, and 100 µg/mL
707 acetylated BSA) was flushed into the flow cell and incubated for 10 minutes. Streptavidin-
708 coated polystyrene beads (0,44 µm in diameter) diluted in buffer B were introduced into the
709 sample chamber and incubated for at least 10 minutes to allow binding to the biotin-labelled
710 DNA ends. Before flushing in the protein in buffer C (20 mM HEPES (pH 7.9), 60 mM KCl,
711 and 0.2% (w/v) BGB), the flow cell was washed twice with buffer C to remove free beads.
712 Finally the flow cell was sealed, followed by incubation with protein or experimental buffer for
713 10 minutes. The measurements were started after 6 minutes of further incubation of the flow
714 cell at a constant temperature of 25 °C. More than 300 beads were measured for each
715 individual experiment. All experiments were performed at least in duplicate.

716 The analysis of the TPM data was performed as previously described [78]. Equation
717 1 was used to calculate the RMS of the individual beads.

718 $$RMS = \sqrt{\frac{1}{n}\sum_{i=1}^{n}[\,(x_i - \overline{x})^2 + (y_i - \overline{y})^2]} \qquad \text{Equation 1}$$

719 where x and y are the coordinates of the beads, $\overline{x}$ and $\overline{y}$ are averaged over the full-time
720 trace. The RMS value of each measured condition was acquired by fitting a Gaussian to the
721 histogram of the RMS values of individual beads.

722

723 All the pictures were prepared for publication in CorelDRAW X8 (Corel).

Acknowledgements

Work in the group of WKS is supported by a Vidi Fellowship (864.10.003) of the Netherlands Organization for Scientific Research (NWO) and a Gisela Their Fellowship from the Leiden University Medical Center. Work in the group of RTD is supported by a VICI grant (016.160.613) of the Netherlands Organization for Scientific Research (NWO), Human Frontier Science Program [RGP0014/2014] and a China Scholarship Council to L.Q. [201506880001]. The authors thank Jeroen Corver for helpful discussions and Patricia Amaral for her assistance with the graphical abstract.

Conflict of interest

WKS has performed research for Cubist. The company had no role in the design or interpretation of these experiments or the decision to publish. Others: none to declare.

739 **References**

740 [1] Lawson PA, Citron DM, Tyrrell KL, Finegold SM. Reclassification of Clostridium difficile as
741 Clostridioides difficile (Hall and O'Toole 1935) Prevot 1938. Anaerobe. 2016;40:95-9.
742 [2] Hensgens MP, Keessen EC, Squire MM, Riley TV, Koene MG, de Boer E, et al. Clostridium difficile
743 infection in the community: a zoonotic disease? Clin Microbiol Infect. 2012;18:635-45.
744 [3] Warriner K, Xu C, Habash M, Sultan S, Weese SJ. Dissemination of Clostridium difficile in food and
745 the environment: Significant sources of C. difficile community-acquired infection? J Appl Microbiol.
746 2017;122:542-53.
747 [4] Smits WK, Lyras D, Lacy DB, Wilcox MH, Kuijper EJ. Clostridium difficile infection. Nat Rev Dis
748 Prim. 2016;2:16020.
749 [5] Crobach MJT, Vernon JJ, Loo VG, Kong LY, Pechine S, Wilcox MH, et al. Understanding Clostridium
750 difficile Colonization. Clin Microbiol Rev. 2018;31.
751 [6] Pituch H. Clostridium difficile is no longer just a nosocomial infection or an infection of adults. Int
752 J Antimicrob Agents. 2009;33 Suppl 1:S42-5.
753 [7] Spigaglia P. Recent advances in the understanding of antibiotic resistance in Clostridium difficile
754 infection. Ther Adv Infect Dis. 2016;3:23-42.
755 [8] Peng Z, Jin D, Kim HB, Stratton CW, Wu B, Tang YW, et al. Update on Antimicrobial Resistance in
756 Clostridium difficile: Resistance Mechanisms and Antimicrobial Susceptibility Testing. J Clin
757 Microbiol. 2017;55:1998-2008.
758 [9] Ehmann DE, Lahiri SD. Novel compounds targeting bacterial DNA topoisomerase/DNA gyrase.
759 Curr Opin Pharmacol. 2014;18:76-83.
760 [10] Bhowmick T, Ghosh S, Dixit K, Ganesan V, Ramagopal UA, Dey D, et al. Targeting Mycobacterium
761 tuberculosis nucleoid-associated protein HU with structure-based inhibitors. Nature
762 communications. 2014;5:4124.
763 [11] van Eijk E, Wittekoek B, Kuijper EJ, Smits WK. DNA replication proteins as potential targets for
764 antimicrobials in drug-resistant bacterial pathogens. J Antimicrob Chemother. 2017;72:1275-84.
765 [12] Wang JC. Cellular roles of DNA topoisomerases: a molecular perspective. Nat Rev Mol Cell Biol.
766 2002;3:430-40.
767 [13] Pelletier J, Halvorsen K, Ha BY, Paparcone R, Sandler SJ, Woldringh CL, et al. Physical
768 manipulation of the Escherichia coli chromosome reveals its soft nature. Proc Natl Acad Sci U S A.
769 2012;109:E2649-56.
770 [14] Zimmerman SB, Murphy LD. Macromolecular crowding and the mandatory condensation of
771 DNA in bacteria. FEBS Lett. 1996;390:245-8.
772 [15] Dame RT, Tark-Dame M. Bacterial chromatin: converging views at different scales. Current
773 Opinion in Cell Biology. 2016;40:60-5.
774 [16] Dillon SC, Dorman CJ. Bacterial nucleoid-associated proteins, nucleoid structure and gene
775 expression. Nat Rev Microbiol. 2010;8:185-95.
776 [17] Ohniwa RL, Ushijima Y, Saito S, Morikawa K. Proteomic analyses of nucleoid-associated proteins
777 in Escherichia coli, Pseudomonas aeruginosa, Bacillus subtilis, and Staphylococcus aureus. PloS one.
778 2011;6:e19172.
779 [18] Grove A. Functional evolution of bacterial histone-like HU proteins. Curr Issues Mol Biol.
780 2011;13:1-12.
781 [19] Kamashev D, Agapova Y, Rastorguev S, Talyzina AA, Boyko KM, Korzhenevskiy DA, et al.
782 Comparison of histone-like HU protein DNA-binding properties and HU/IHF protein sequence
783 alignment. PloS one. 2017;12:e0188037.
784 [20] Boubrik F, Bonnefoy E, Rouviere-Yaniv J. HU and IHF: similarities and differences. In Escherichia
785 coli, the lack of HU is not compensated for by IHF. Res Microbiol. 1991;142:239-47.
786 [21] Claret L, Rouviere-Yaniv J. Variation in HU composition during growth of Escherichia coli: the
787 heterodimer is required for long term survival. Journal of molecular biology. 1997;273:93-104.

788 [22] Guo F, Adhya S. Spiral structure of Escherichia coli HUalphabeta provides foundation for DNA
789 supercoiling. Proc Natl Acad Sci U S A. 2007;104:4309-14.
790 [23] Kohler P, Marahiel MA. Association of the histone-like protein HBsu with the nucleoid of Bacillus
791 subtilis. Journal of bacteriology. 1997;179:2060-4.
792 [24] Giangrossi M, Giuliodori AM, Gualerzi CO, Pon CL. Selective expression of the beta-subunit of
793 nucleoid-associated protein HU during cold shock in Escherichia coli. Mol Microbiol. 2002;44:205-16.
794 [25] Painbeni E, Caroff M, Rouviere-Yaniv J. Alterations of the outer membrane composition in
795 Escherichia coli lacking the histone-like protein HU. Proc Natl Acad Sci U S A. 1997;94:6712-7.
796 [26] van Noort J, Verbrugge S, Goosen N, Dekker C, Dame RT. Dual architectural roles of HU:
797 formation of flexible hinges and rigid filaments. Proc Natl Acad Sci U S A. 2004;101:6969-74.
798 [27] Dame RT, Hall MA, Wang MD. Single-molecule unzipping force analysis of HU-DNA complexes.
799 Chembiochem. 2013;14:1954-7.
800 [28] Balandina A, Kamashev D, Rouviere-Yaniv J. The bacterial histone-like protein HU specifically
801 recognizes similar structures in all nucleic acids. DNA, RNA, and their hybrids. J Biol Chem.
802 2002;277:27622-8.
803 [29] Grainger DC, Hurd D, Goldberg MD, Busby SJ. Association of nucleoid proteins with coding and
804 non-coding segments of the Escherichia coli genome. Nucleic Acids Res. 2006;34:4642-52.
805 [30] Navarre WW, Porwollik S, Wang Y, McClelland M, Rosen H, Libby SJ, et al. Selective silencing of
806 foreign DNA with low GC content by the H-NS protein in Salmonella. Science. 2006;313:236-8.
807 [31] Gordon BR, Li Y, Cote A, Weirauch MT, Ding P, Hughes TR, et al. Structural basis for recognition
808 of AT-rich DNA by unrelated xenogeneic silencing proteins. Proc Natl Acad Sci U S A.
809 2011;108:10690-5.
810 [32] Kohler P, Marahiel MA. Mutational analysis of the nucleoid-associated protein HBsu of Bacillus
811 subtilis. Mol Gen Genet. 1998;260:487-91.
812 [33] Bensaid A, Almeida A, Drlica K, Rouviere-Yaniv J. Cross-talk between topoisomerase I and HU in
813 Escherichia coli. Journal of molecular biology. 1996;256:292-300.
814 [34] Dame RT, Goosen N. HU: promoting or counteracting DNA compaction? FEBS Lett.
815 2002;529:151-6.
816 [35] Swinger KK, Lemberg KM, Zhang Y, Rice PA. Flexible DNA bending in HU-DNA cocrystal
817 structures. EMBO J. 2003;22:3749-60.
818 [36] Aki T, Choy HE, Adhya S. Histone-like protein HU as a specific transcriptional regulator: co-factor
819 role in repression of gal transcription by GAL repressor. Genes Cells. 1996;1:179-88.
820 [37] Morales P, Rouviere-Yaniv J, Dreyfus M. The histone-like protein HU does not obstruct
821 movement of T7 RNA polymerase in Escherichia coli cells but stimulates its activity. Journal of
822 bacteriology. 2002;184:1565-70.
823 [38] Oberto J, Nabti S, Jooste V, Mignot H, Rouviere-Yaniv J. The HU regulon is composed of genes
824 responding to anaerobiosis, acid stress, high osmolarity and SOS induction. PloS one. 2009;4:e4367.
825 [39] Priyadarshini R, Cugini C, Arndt A, Chen T, Tjokro NO, Goodman SD, et al. The nucleoid-
826 associated protein HUbeta affects global gene expression in Porphyromonas gingivalis. Microbiology.
827 2013;159:219-29.
828 [40] Berger M, Farcas A, Geertz M, Zhelyazkova P, Brix K, Travers A, et al. Coordination of genomic
829 structure and transcription by the main bacterial nucleoid-associated protein HU. EMBO reports.
830 2010;11:59-64.
831 [41] Lewis DEA, Geanacopoulos M, Adhya S. Role of HU and DNA supercoiling in transcription
832 repression: specialized nucleoprotein repression complex at gal promoters in Escherichia coli.
833 Molecular Microbiology. 1999;31:451-61.
834 [42] Chodavarapu S, Felczak MM, Yaniv JR, Kaguni JM. Escherichia coli DnaA interacts with HU in
835 initiation at the E. coli replication origin. Mol Microbiol. 2008;67:781-92.
836 [43] Jaffe A, Vinella D, D'Ari R. The Escherichia coli histone-like protein HU affects DNA initiation,
837 chromosome partitioning via MukB, and cell division via MinCDE. Journal of bacteriology.
838 1997;179:3494-9.

839 [44] Mangan MW, Lucchini S, T OC, Fitzgerald S, Hinton JC, Dorman CJ. Nucleoid-associated protein
840 HU controls three regulons that coordinate virulence, response to stress and general physiology in
841 Salmonella enterica serovar Typhimurium. Microbiology. 2011;157:1075-87.
842 [45] Alvarez A, Toledo H. The histone-like protein HU has a role in gene expression during the acid
843 adaptation response in Helicobacter pylori. Helicobacter. 2017;22.
844 [46] Sakatos A, Babunovic GH, Chase MR, Dills A, Leszyk J, Rosebrock T, et al. Posttranslational
845 modification of a histone-like protein regulates phenotypic resistance to isoniazid in mycobacteria.
846 Sci Adv. 2018;4:eaao1478.
847 [47] Ferrandiz MJ, Carreno D, Ayora S, de la Campa AG. HU of Streptococcus pneumoniae Is Essential
848 for the Preservation of DNA Supercoiling. Front Microbiol. 2018;9:493.
849 [48] Sebaihia M, Wren BW, Mullany P, Fairweather NF, Minton N, Stabler R, et al. The multidrug-
850 resistant human pathogen Clostridium difficile has a highly mobile, mosaic genome. Nature genetics.
851 2006;38:779-86.
852 [49] Dembek M, Barquist L, Boinett CJ, Cain AK, Mayho M, Lawley TD, et al. High-throughput analysis
853 of gene essentiality and sporulation in Clostridium difficile. MBio. 2015;6:e02383.
854 [50] Swinger KK, Rice PA. Structure-based analysis of HU-DNA binding. Journal of molecular biology.
855 2007;365:1005-16.
856 [51] Kelley LA, Mezulis S, Yates CM, Wass MN, Sternberg MJ. The Phyre2 web portal for protein
857 modeling, prediction and analysis. Nat Protoc. 2015;10:845-58.
858 [52] Waterhouse A, Bertoni M, Bienert S, Studer G, Tauriello G, Gumienny R, et al. SWISS-MODEL:
859 homology modelling of protein structures and complexes. Nucleic Acids Res. 2018.
860 [53] Kim DH, Im H, Jee JG, Jang SB, Yoon HJ, Kwon AR, et al. beta-Arm flexibility of HU from
861 Staphylococcus aureus dictates the DNA-binding and recognition mechanism. Acta Crystallogr D Biol
862 Crystallogr. 2014;70:3273-89.
863 [54] Hammel M, Amlanjyoti D, Reyes FE, Chen JH, Parpana R, Tang HY, et al. HU multimerization shift
864 controls nucleoid compaction. Sci Adv. 2016;2:e1600650.
865 [55] Mouw KW, Rice PA. Shaping the Borrelia burgdorferi genome: crystal structure and binding
866 properties of the DNA-bending protein Hbb. Mol Microbiol. 2007;63:1319-30.
867 [56] Kamau E, Tsihlis ND, Simmons LA, Grove A. Surface salt bridges modulate the DNA site size of
868 bacterial histone-like HU proteins. Biochem J. 2005;390:49-55.
869 [57] Saitoh F, Kawamura S, Yamasaki N, Tanaka I, Kimura M. Arginine-55 in the beta-arm is essential
870 for the activity of DNA-binding protein HU from Bacillus stearothermophilus. Biosci Biotechnol
871 Biochem. 1999;63:2232-5.
872 [58] Goshima N, Kohno K, Imamoto F, Kano Y. HU-1 mutants of Escherichia coli deficient in DNA
873 binding. Gene. 1990;96:141-5.
874 [59] Smits WK, Grossman AD. The transcriptional regulator Rok binds A+T-rich DNA and is involved in
875 repression of a mobile genetic element in Bacillus subtilis. PLoS Genet. 2010;6:e1001207.
876 [60] Seco EM, Ayora S. Bacillus subtilis DNA polymerases, PolC and DnaE, are required for both
877 leading and lagging strand synthesis in SPP1 origin-dependent DNA replication. Nucleic acids
878 research. 2017;45:8302-13.
879 [61] Dixon AS, Schwinn MK, Hall MP, Zimmerman K, Otto P, Lubben TH, et al. NanoLuc
880 Complementation Reporter Optimized for Accurate Measurement of Protein Interactions in Cells.
881 ACS Chem Biol. 2016;11:400-8.
882 [62] Oliveira Paiva AM, Friggen AH, Hossein-Javaheri S, Smits WK. The Signal Sequence of the
883 Abundant Extracellular Metalloprotease PPEP-1 Can Be Used to Secrete Synthetic Reporter Proteins
884 in Clostridium difficile. ACS Synth Biol. 2016.
885 [63] Fagan RP, Fairweather NF. Clostridium difficile has two parallel and essential Sec secretion
886 systems. Journal of Biological Chemistry. 2011;286:27483-93.
887 [64] van Eijk E, Anvar SY, Browne HP, Leung WY, Frank J, Schmitz AM, et al. Complete genome
888 sequence of the Clostridium difficile laboratory strain 630Deltaerm reveals differences from strain
889 630, including translocation of the mobile element CTn5. BMC genomics. 2015;16:31.

890 [65] Los GV, Encell LP, McDougal MG, Hartzell DD, Karassina N, Zimprich C, et al. HaloTag: A Novel
891 Protein Labeling Technology for Cell Imaging and Protein Analysis. American Chemical Society. 2010.
892 [66] Stagge F, Mitronova GY, Belov VN, Wurm CA, Jakobs S. SNAP-, CLIP- and Halo-tag labelling of
893 budding yeast cells. PLoS One. 2013;8:e78745.
894 [67] Ke N, Landgraf D, Paulsson J, Berkmen M. Visualization of Periplasmic and Cytoplasmic Proteins
895 with a Self-Labeling Protein Tag. Journal of bacteriology. 2016;198:1035-43.
896 [68] Cassona CP, Pereira F, Serrano M, Henriques AO. A Fluorescent Reporter for Single Cell Analysis
897 of Gene Expression in Clostridium difficile. Methods Mol Biol. 2016;1476:69-90.
898 [69] Buckley AM, Jukes C, Candlish D, Irvine JJ, Spencer J, Fagan RP, et al. Lighting Up Clostridium
899 Difficile: Reporting Gene Expression Using Fluorescent Lov Domains. Sci Rep. 2016;6:23463.
900 [70] Ransom EM, Ellermeier CD, Weiss DS. Use of mCherry Red fluorescent protein for studies of
901 protein localization and gene expression in Clostridium difficile. Applied and environmental
902 microbiology. 2015;81:1652-60.
903 [71] Wery M, Woldringh CL, Rouviere-Yaniv J. HU-GFP and DAPI co-localize on the Escherichia coli
904 nucleoid. Biochimie. 2001;83:193-200.
905 [72] Holowka J, Trojanowski D, Ginda K, Wojtas B, Gielniewski B, Jakimowicz D, et al. HupB Is a
906 Bacterial Nucleoid-Associated Protein with an Indispensable Eukaryotic-Like Tail. MBio. 2017;8.
907 [73] Ransom EM, Williams KB, Weiss DS, Ellermeier CD. Identification and characterization of a gene
908 cluster required for proper rod shape, cell division, and pathogenesis in Clostridium difficile. Journal
909 of bacteriology. 2014;196:2290-300.
910 [74] Binder D, Probst C, Grunberger A, Hilgers F, Loeschcke A, Jaeger KE, et al. Comparative Single-
911 Cell Analysis of Different E. coli Expression Systems during Microfluidic Cultivation. PloS one.
912 2016;11:e0160711.
913 [75] Jin DJ, Cagliero C, Zhou YN. Role of RNA polymerase and transcription in the organization of the
914 bacterial nucleoid. Chem Rev. 2013;113:8662-82.
915 [76] Hodges-Garcia Y, Hagerman PJ, Pettijohn DE. DNA ring closure mediated by protein HU. J Biol
916 Chem. 1989;264:14621-3.
917 [77] Driessen RP, Sitters G, Laurens N, Moolenaar GF, Wuite GJ, Goosen N, et al. Effect of
918 temperature on the intrinsic flexibility of DNA and its interaction with architectural proteins.
919 Biochemistry. 2014;53:6430-8.
920 [78] van der Valk RA, Laurens N, Dame RT. Tethered Particle Motion Analysis of the DNA Binding
921 Properties of Architectural Proteins. Methods Mol Biol. 2017;1624:127-43.
922 [79] Skoko D, Wong B, Johnson RC, Marko JF. Micromechanical analysis of the binding of DNA-
923 bending proteins HMGB1, NHP6A, and HU reveals their ability to form highly stable DNA-protein
924 complexes. Biochemistry. 2004;43:13867-74.
925 [80] Xiao B, Johnson RC, Marko JF. Modulation of HU-DNA interactions by salt concentration and
926 applied force. Nucleic acids research. 2010;38:6176-85.
927 [81] Lioy VS, Cournac A, Marbouty M, Duigou S, Mozziconacci J, Espeli O, et al. Multiscale Structuring
928 of the E. coli Chromosome by Nucleoid-Associated and Condensin Proteins. Cell. 2018;172:771-83
929 e18.
930 [82] Le TB, Imakaev MV, Mirny LA, Laub MT. High-resolution mapping of the spatial organization of a
931 bacterial chromosome. Science. 2013;342:731-4.
932 [83] Sievers F, Wilm A, Dineen D, Gibson TJ, Karplus K, Li W, et al. Fast, scalable generation of high-
933 quality protein multiple sequence alignments using Clustal Omega. Mol Syst Biol. 2011;7:539.
934 [84] Jurrus E, Engel D, Star K, Monson K, Brandi J, Felberg LE, et al. Improvements to the APBS
935 biomolecular solvation software suite. Protein Sci. 2018;27:112-28.
936 [85] Sambrook J, Fritsch EF, Maniatis T. Molecular cloning : a laboratory manual. Cold Spring Harbor,
937 N.Y.: Cold Spring Harbor Laboratory; 1989.
938 [86] Purdy D, O'Keeffe TAT, Elmore M, Herbert M, McLeod A, Bokori-Brown M, et al. Conjugative
939 transfer of clostridial shuttle vectors from Escherichia coli to Clostridium difficile through
940 circumvention of the restriction barrier. Molecular Microbiology. 2002;46:439-52.

941 [87] Hussain HA, Roberts AP, Mullany P. Generation of an erythromycin-sensitive derivative of
942 Clostridium difficile strain 630 (630Deltaerm) and demonstration that the conjugative transposon
943 Tn916DeltaE enters the genome of this strain at multiple sites. J Med Microbiol. 2005;54:137-41.
944 [88] Gibson DG. Enzymatic assembly of overlapping DNA fragments. Methods Enzymol.
945 2011;498:349-61.
946 [89] Laurent TC, Killander J. A theory of gel filtration and its exeperimental verification. Journal of
947 Chromatography A. 1964;14:317-30.
948 [90] Ducret A, Quardokus EM, Brun YV. MicrobeJ, a tool for high throughput bacterial cell detection
949 and quantitative analysis. Nat Microbiol. 2016;1:16077.
950 [91] Rueden CT, Schindelin J, Hiner MC, DeZonia BE, Walter AE, Arena ET, et al. ImageJ2: ImageJ for
951 the next generation of scientific image data. BMC Bioinformatics. 2017;18:529.
952 [92] Driessen RP, Lin SN, Waterreus WJ, van der Meulen AL, van der Valk RA, Laurens N, et al.
953 Diverse architectural properties of Sso10a proteins: Evidence for a role in chromatin compaction and
954 organization. Sci Rep. 2016;6:29422.

955

956

Table 1. Plasmids used in this study.

Name	Relevant features *	Source/Reference
pH6HTC	$P_{T7,}$ HaloTag-His6, *amp*	Promega
pCR2.1-TOPO	TA vector; pMB1 oriR; *km amp*	ThermoFisher
pET28b	$lacI^{q}$, P_{T7} expression vector, *km*	Novagen
pRPF185	*tetR* P_{tet}-*gusA*; *catP*	[65]
pAP24	*tetR* P_{tet}-$sLuc^{opt}$; *catP*	[64]
pRD118	P_{T7}-s*so685*	[92]
pAF226	P_{T7}-$hupA_{6xHis}$; *km*	This study
pAF232	P_{T7}-$hupA^{QE}{}_{6xHis}$; *km*	This study
pAF234	P_{T7}-$hupA^{QED}{}_{6xHis}$; *km*	This study
pAF235	*tetR* P_{tet}-$hupA^{QE}$-$HaloTag_{6xHis}$; *catP*	This study
pAF237	*tetR* P_{tet}-$hupA^{QED}$-$HaloTag_{6xHis}$; *catP*	This study
pAF254	*tetR* P_{tet}-luc^{opt}; *catP*	This study
pAF255	*tetR* P_{tet}-*lgbit*; *catP*	This study
pAF256	*tetR* P_{tet}-*hupA-smbit*/*lgbit*; *catP*	This study
pAF257	*tetR* P_{tet}-*smBit*/*hupA-lgbit*; *catP*	This study
pAF259	*tetR* P_{tet}-$bitluc^{opt}$; *catP*	This study
pAF260	*tetR* P_{tet}-*smbit*; *catP*	This study
pAF262	*tetR* P_{tet}-*smbit/lgbit*; *catP*	This study
pAP103	*tetR* P_{tet}-*hupA*; *catP*	This study
pAP118	*tetR* P_{tet}-*hupA-smbit*/*hupA-lgbit*; *catP*	This study
pAP134	*tetR* P_{tet}-*hupA-lgbit*; *catP*	This study
pAP135	*tetR* P_{tet}-*hupA-smbit*; *catP*	This study
pAP159	*tetR* P_{tet}-*sbit/lgbit* (GTT); *catP*	This study
pAP210	*tetR* P_{tet}-$hupA^{QED}$-*smbit*/*hupA-lgbit*; *catP*	This study
pRD4	*tetR* P_{tet}-*hupA*-$HaloTag_{6xHis}$; *catP*	This study
pWKS1744	pCR2.1-TOPO with *hupA; km amp*	This study
pWKS1746	pCR2.1-TOPO with $HaloTag_{6xHis}$*; km amp*	This study

* *amp* – ampicillin resistance cassette *catP* – chloramphenicol resistance cassette, *km* – kanamycin resistance cassette

Table 2. *C. difficile* strains used in this study.

Name	Relevant Genotype/Phenotype*	Source/Reference
AP6	*C. difficile 630Δerm*; Erm^S	[66, 87]
WKS1588	*630Δerm* pRPF185; $Thia^R$	This study
RD16	*630Δerm* pRD4; $Thia^R$	This study
AF239	*630Δerm* pAF237; $Thia^R$	This study
AP34	*630Δerm* pAP24; $Thia^R$	[64]
AP106	*630Δerm* pAP103; $Thia^R$	This study
AP122	*630Δerm* pAP118; $Thia^R$	This study
AP152	*630Δerm* pAP134; $Thia^R$	This study
AP153	*630Δerm* pAP135; $Thia^R$	This study
AP181	*630Δerm* pAF254; $Thia^R$	This study
AP182	*630Δerm* pAF259; $Thia^R$	This study
AP183	*630Δerm* pAF256; $Thia^R$	This study
AP184	*630Δerm* pAF257; $Thia^R$	This study
AP199	*630Δerm* pAF255; $Thia^R$	This study
AP201	*630Δerm* pAF260; $Thia^R$	This study
AP202	*630Δerm* pAF262; $Thia^R$	This study
AP212	*630Δerm* pAP210; $Thia^R$	This study

* Erm^S – Erythromycin sensitive, $Thia^R$ – Thiamphenicol resistant

Table 3. Oligonucleotides used in this study.

Name	Sequence (5'>3') *
oAF57	GTCGCCATGGATGAATAAAGCTGAATTAGTATCAAAG
oAF58	GACGCTCGAGTCCATTTATTATATCCTTTAATCC
oAF61	CGCCAGGCCAGGGCTGTCACTGTGCAGCTCGTGGACGC
oAF62	GCGTCCACGAGCTGCACAGTGACAGCCCTGGCCTGGCG
oAF63	CATCAGGCAAGAGTAGTCACTGTGTAGCTCGTGGATGC
oAF64	GCATCCACGAGCTACACAGTGACTACTCTTGCCTGATG
oAF65	CATTAAGTATGAGTATTCTATGTATAGATCATTGATGC
oAF66	GCATCAATGATCTATACATAGAATACTCATACTTAATG
oAF73	CATTTGAGACAAGAGAACAGGCTGCTGAACAAGGAAGAAATCCAAGAG
oAF74	CTTGGATTTCTTCCTTGTTCAGCAGCCTGTTCTCTTGTCTCAAATGTTC
oAF75	GGCTGCTGAACAAGGAGATAATCCAAGAGATCCAGAGC
oAF76	CTGGATCTCTTGGATTATCTCCTTGTTCAGCAGCCTG
oAF81	GCTAGAATTCGCCACTGGCAGCAGCCAC
oAF82	CCTAGAATTCCTGTCCTTCTAGTGTAGCCG
oAP47	TAGGATCCTTATCCATTTATTATATCCTTTAATCC
oAP48	CT GAGCTCCTGCAGTAAAGGAGAAAATTTTGTTTTTACACTTGAAGATTTTGTGG
oAP49	TAGGATCCCTATGCTAGAATACGTTCAC
oAP54	CTGAGCTCCTGCAGTAAAGGAGAAAATTTTGTTTTTACACTTGAAGATTTTGTG
oAP55	TAGGATCCCTATAGAATTTCTTCAAAAAGTCTATAACCTGTAACACTGTTTATAGTTAC
oAP58	GGATCCTATAAGTTTTAATAAAACTTTAAATAG
oAP59	AGCTCAGATCTGTTAACGCTACGATCAAGC
oAP60	GCTTGATCGTAGCGTTAACAGATCTGAGC
oAP61	CTCCTTTACTGCAGCGATCGAGCTATAG
oAP62	GAAGAAATTCTATAGCTCGATCGCTGCAG
oAP63	GTTTTATTAAAACTTATAGGATCCCTAACTGTTTATAG
oAP64	GATCTGAGCTCCTGCAGTAAAGGAGAAAATTTTGTGAATAAAGC
oAP65	CTTATAGGATCCAGCTATAGAATTTCTTC
oAP66	GATCTGAGCTCCTGCAGTAAAGGAGAAAATTTTGTTACAGGTTATAGAC
oAP67	GCTCGATCGCTGCAGTAAAGGAGAAAATTTTGTTTTTACACTTGAAGATTTTGTG
oAP96	GCAGTAAAGGAGAAAATTTTGTGTTTACACTTGAAGATTTTG
oAP97	CACAAAATCTTCAAGTGTAAACACAAAATTTTCTCCTTTAC
oAP98	GCAGTAAAGGAGAAAATTTTGTGACAGGTTATAGACTTTTTG
oAP99	CTTCAAAAAGTCTATAACCTGTCACAAAATTTTCTCCTTTAC
oAP110	CCCCTCGAGATCCATTTATTATATCCTTTAATCC
oRD5	CAGGATCTGGTTCAGGAAGTCTCGAGGGTTCCGAAATCGGTACTGG
Sso10a-2Nde	ATACATATGCAACTTGAACGGCGTAAAAGAGGAACAATGG
Sso10a-2Bam685	GGTGGATCCTTTTCATCCCTTTAGTTCTTCCAG
oWKS-1511	CTCGAGTCAGGATCTGGTTCAGGAAGTGGTTCCGAAATCGGTACTGGCTTTCC
oWKS-1512	GGATCCTTAGTGGTGATGGTGATGATGACC
oWKS-1519	GAGCTCAAATTTGAATTTTTTAGGGGGAAAATACCGTGAATAAAGCTGAATTAGTATCAAAG
oWKS-1520	CTCGAGACTTCCTGAACCAGATCCTGATCCATTTATTATATCCTTTAATCCTTTTC

* Restriction enzyme sites used underlined

Legends

Fig. 1. *Clostridium difficile* HupA is a homologue of bacterial HU proteins. (a) Multiple sequence alignment (ClustalOmega) of *C. difficile* HupA with homologous proteins from the Uniprot database. The protein sequences from *C. difficile* 630Δ*erm* (Q180Z4), *Escherichia coli* αHU (P0ACF0), *E. coli* βHU (P0ACF4), *Bacillus subtilis* (A3F3E2), *Geobacillus stearothermophilus* (P0A3H0), *Bacillus anthracis* (Q81WV7), *Staphylococcus aureus* (Q99U17), *Salmonella typhimurium* (P0A1R8), *Streptococcus pneumoniae* (AAK75224), *Streptococcus mutans* (Q9XB21), *Mycobacterium tuberculosis* (P9WMK7), *Thermotoga. maritima* (P36206) and *Anabaena sp.* (P05514) were selected for alignment. Residues are coloured according to ClustalW2 convention. Conserved residues (indicated with symbols below the alignment) are additionally highlighted with grey shading (darker = more conserved), except for the three arginine residues that were subjected to mutagenesis (in bold), that are highlighted in blue. (b) Structural model of the *C. difficile* HupA dimer based on homology with the crystal structure of DNA-bound nucleoid associated protein SAV1473 (SWISS-MODEL, PDB: 4QJN, 58.43% identity). α-helixes are represented in red, β-sheets in orange and unstructured regions in grey. Both the N-terminus and the C-terminus are indicated in the figure. A DNA binding pocket is formed by the arm regions of the dimer, composed by 4 β-sheets in each monomer. The localization of the substituted residues (R55, R58 and R61) are indicated (blue, sticks). (c) Electrostatic surface potential of *C. difficile* HupA. The electrostatic potential is in eV with the range shown in the corresponding color bar.

Fig. 2 – Dimerization of HupA is independent of DNA binding. (a) Electrophoretic mobility shift assays with increasing concentrations (0.25 -2 μM) of $HupA_{6xHis}$ and $HupA^{QED}{}_{6xHis}$. Gel shift assays were performed with 2.4 nM radio-labeled ([γ-^{32}P] ATP) 29% G+C dsDNA oligonucleotide incubated with HupA for 20 min at room temperature prior to separation. Protein-DNA complexes were analysed on native 8% polyacrylamide gels, vacuum-dried and

visualized by phosphorimaging. ssDNA and dsDNA (without protein added, "-") were used as controls. (b) Quantification of the gel-shift DNA-protein complex by densitometry. Gel shift assays were performed with 2.4 nM radio labelled ([ɣ-^{32}P] ATP) dsDNA oligonucleotides with different 29-71% G+C content and the indicated concentration of $HupA_{6xHis}$ (red) and $HupA^{QED}{}_{6xHis}$ (blue). (c) Elution profiles of $HupA_{6xHis}$ (red) and $HupA^{QED}{}_{6xHis}$ (blue) from size exclusion chromatography. The experiments were performed with purified protein (100 µM) on a Superdex HR 75 10/30 column. The elution position of protein standards of the indicated MW (in kDa) are indicated by vertical grey dashed lines. The elution profiles show a single peak, corresponding to a ~38 kDa multimer, when compared to the predicted molecular weight of the monomer (11 kDa). No significant difference in the elution profile of the $HupA^{QED}{}_{6xHis}$ compared to $HupA_{6xHis}$ was observed. (d) Western-blot analysis of glutaraldehyde cross-linking of $HupA_{6xHis}$ and $HupA^{QED}{}_{6xHis}$. 100 ng HupA was incubated with 0%, 0.0006% and 0.006% glutaraldehyde for 30 min at room temperature. The samples were resolved by SDS-PAGE and analysed by immunoblotted with anti-his antibody. Crosslinking between the HupA monomers is observed with the approximate molecular weight of a homo-dimer (~22 kDa). Additional bands of lower molecular weight HupA are observed (*) that likely represent breakdown products.

Fig. 3 – HupA demonstrates self-interaction in *C. difficile*. A split luciferase complementation assay was used to demonstrate interactions between HupA monomers *in vivo*. Cells were induced with 200 ng/mL anhydrotetracycline (ATc) for 60 min. Optical density-normalized luciferase activity (LU/OD) is shown right before induction (T0, blue bars) and after 1 hour of induction (T1, red bars). The averages of biological triplicate measurements are shown, with error bars indicating the standard deviation from the mean. Luciferase activity of strains AP182 (P_{tet}-*bitluc^{opt}*), AP122 (P_{tet}-*hupA-smbit/hupA-lgbit*), AP152 (P_{tet}-*hupA-lgbit*), AP153 (P_{tet}-*hupA-smbit*), AP183 (P_{tet}-*hupA-smbit-lgbit*) and AP184 (P_{tet}-*smbit-hupA-lgbit*). A positive interaction was defined on the basis of the negative controls as a luciferase activity of >1000 LU/OD. No

significant difference was detected at T0. AP122 and AP182 were significantly higher with $p<0.0001$ (*) by two-way ANOVA.

Fig. 4 – HupA overexpression leads to compaction of the nucleoid *in vivo*. (a) Fluorescence microscopy analysis of *C. difficile* 630Δ*erm* harboring the vector for anhydrotetracycline (ATc)-dependent overexpression of HupA (AP106). For HupA overexpression, cells were induced at mid-exponential growth in liquid medium with different ATc concentrations (50, 100 and 200 ng/mL) for 1h. *C. difficile* 630Δ*erm* and non-induced AP106 were used as controls. The cells were stained with DAPI for DNA visualization (nucleoid). The nucleoid was false colored in cyan for better contrast. Phase contrast (PC) and an overlay of both channels is shown. Because growth is asynchronous in these conditions, cells representing different cell cycles stages can be found. In the presence of ATc, the chromosome appears more compacted. White arrow indicates the cells with mid-cell nucleoid. Scale bar = 2 µm. (b) Boxplots of mean nucleoid length. Whiskers represent minimum and maximum nucleoid length observed. Black dots represent the mean and the grey lines represent the median values. Quantifications were performed using MicrobeJ from at least two biological replicates for each condition. n is the number of cells analyzed per condition. (c) Boxplots of mean cell length. Whiskers represent minimum and maximum cell length observed. Black dots represent the mean and the grey lines represent the median values. Quantifications were performed using MicrobeJ from at least two biological replicates for each condition. The same cells as analyzed for nucleoid length were used. * $p<0,05$ ** $p<0,0001$ by one-way ANOVA compared to wild type (wt). ns = nonsignificant.

Fig. 5 – HupA co-localizes with the nucleoid. (a) Fluorescence microscopy analysis of *C. difficile* 630Δ*erm* harboring a vector for expression of HupA-HaloTag (RD16) or a vector for expression of $HupA^{QED}$-HaloTag (AF239). For visualization of HupA-HaloTag and $HupA^{QED}$-

HaloTag, cells were induced at mid-exponential growth phase with 200 ng/mL anhydrotetracycline (ATc) for 1h and incubated with Oregon Green HaloTag substrate for 30 min. The cells were stained with DAPI stain to visualize DNA (nucleoid). The nucleoid was false colored in cyan for better contrast. As control non-induced RD16 is shown, but similar results were obtained for non-induced AF239. Phase contrast (PC) and an overlay of the channels is shown. Because growth is asynchronous under these conditions, cells representing different cell cycles stages can be found. In the presence of ATc the chromosome appears more compacted and HupA-HaloTag co-localizes with the nucleoid. Scale bar = 2 µm. (b) Average intensity profile scans for the nucleoid (DAPI, blue line) and HupA fusion protein (Oregon Green, green line) obtained from a MicrobeJ analysis from at least two biological replicates in each condition. 289 cells were analyzed for HupA-HaloTag and 331 cells were analyzed for $HupA^{QED}$-HaloTag. Standard deviation of the mean is represented by the respective color shade. (c) In-gel fluorescent analysis of RD16 and AF239 samples before induction (T0), 1 and 3 hours after induction (T1, T3). Samples were incubated with Oregon Green substrate for 30 min and run on a 12% SDS-PAGE.

Fig. 6 – HupA alters the topology of DNA *in vitro*. (a) Ligase-mediated cyclization assay. A 119 bp [γ-^{32}P]ATP-labelled dsDNA fragment was incubated in the presence of increasing concentrations of $HupA_{6xHis}$ (1, 10 µM), exonuclease III and ligase, as indicated above the panel. The presence of ExoIII-resistant (i.e. circular) DNA fragments is observed when samples are incubated with $HupA_{6xHis}$ ("circle"). (b) The effect of increasing concentrations of HupA (black circles), $HupA_{6xHis}$ (red squares) and $HupA^{QED}{}_{6xHis}$ (blue triangles) on DNA conformation in tethered particle motion experiments. Root mean square (RMS; see Equation 1/Materials and methods) values as a function of protein concentration is shown. Increasing concentrations of HupA and $HupA_{6xHis}$ lead to a decreased RMS, suggesting compaction of the DNA.

Fig. 7 – Strain viability under conditions of HupA overexpression. Spot assay of serially diluted *C. difficile* strains 630Δ*erm,* RD16 (P_{tet}-*hupA-HaloTag*), AF239 (P_{tet}-*hupA*^{QED}-*Halotag*), AP106 (P_{tet}-*hupA*) and AP34 (P_{tet}-*sluc*^{opt}). The left panel shows growth on medium with only *C. difficile* selective supplement (CDSS), the middle panel shows growth on medium with CDSS and thiamphenicol (Thi) and the right panel shows growth on medium with CDSS, Thi and 200 ng/mL anhydrotetracyclin (ATc) after 24 hours at 37ºC. The results were verified by four independent spot assays and a typical image is shown. Overexpression of HupA strongly reduces cell viability.

Figure 1

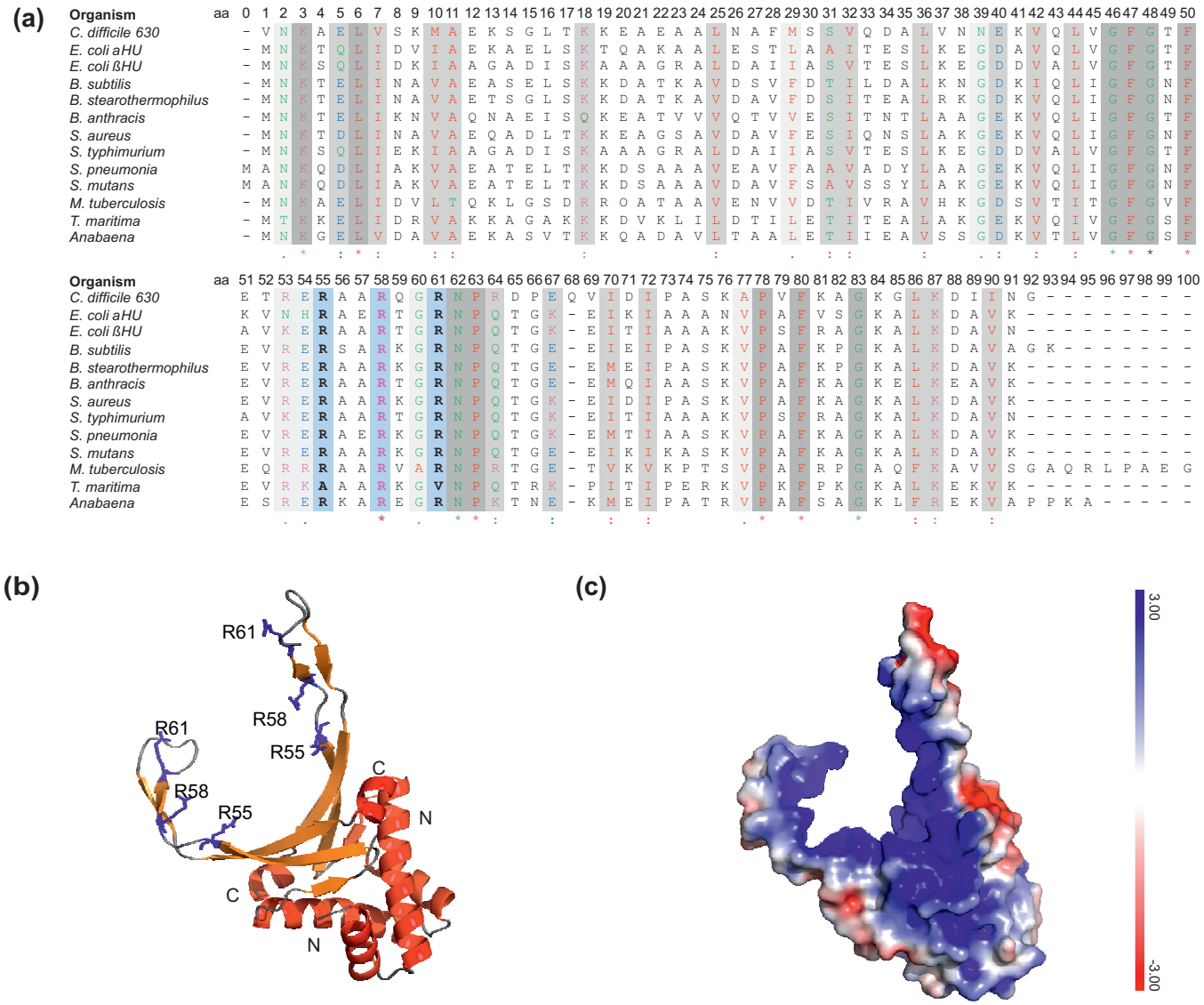
(a)
Organism
aa
C. difficile 630
E. coli aHU
E. coli ßHU
B. subtilis
B. stearothermophilus
B. anthracis
S. aureus
S. typhimurium
S. pneumonia
S. mutans
M. tuberculosis
T. maritima
Anabaena
(b)
R61
R58
R55
C
N
(c)
3.00
-3.00

Figure 2

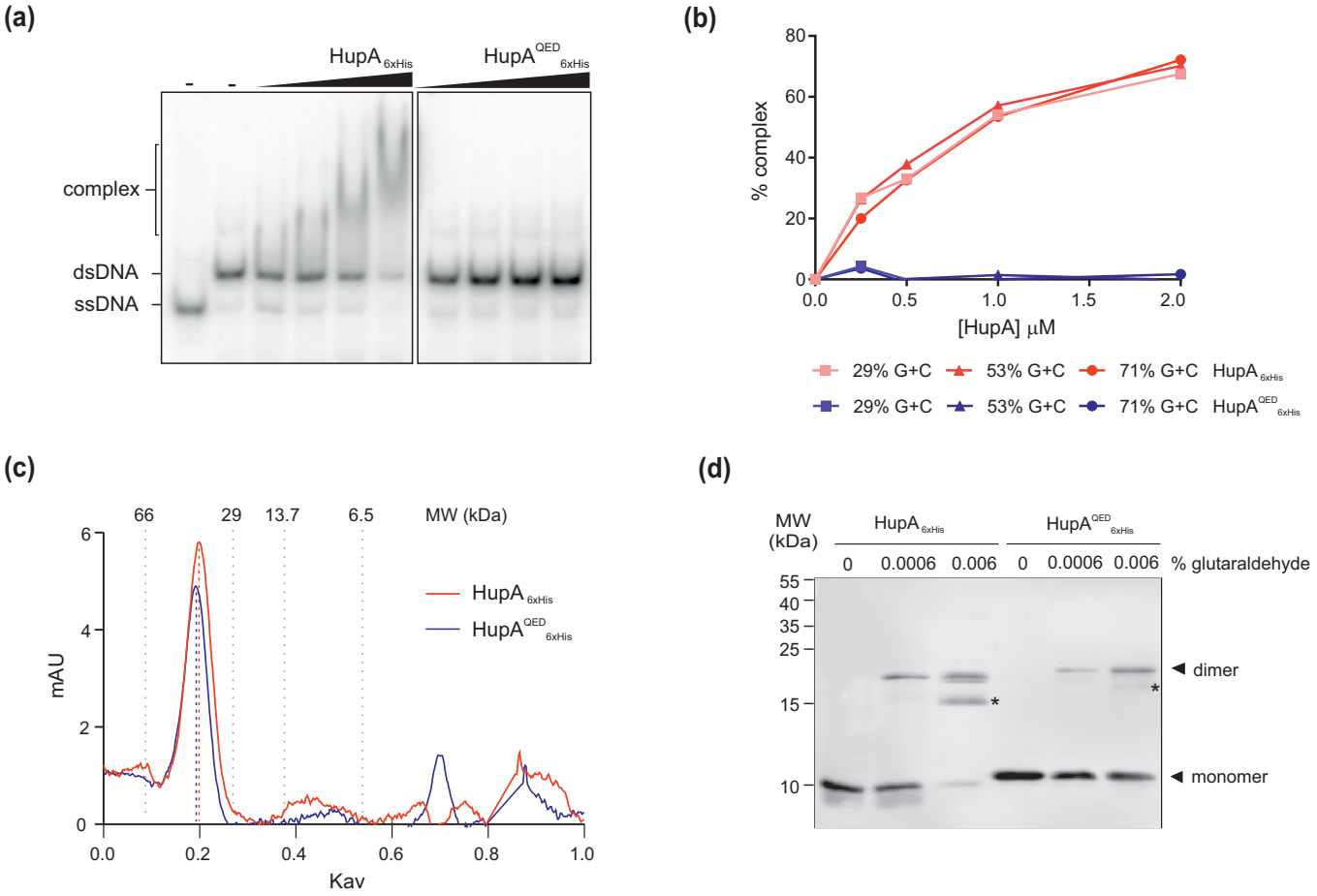
(a)
HupA 6xHis
HupA QED 6xHis
complex
dsDNA
ssDNA
(b)
% complex
[HupA] μM
29% G+C
53% G+C
71% G+C
HupA 6xHis
HupA QED 6xHis
(c)
MW (kDa)
66
29
13.7
6.5
mAU
Kav
HupA 6xHis
HupA QED 6xHis
(d)
MW (kDa)
HupA 6xHis
HupA QED 6xHis
% glutaraldehyde
dimer
monomer

Figure 3

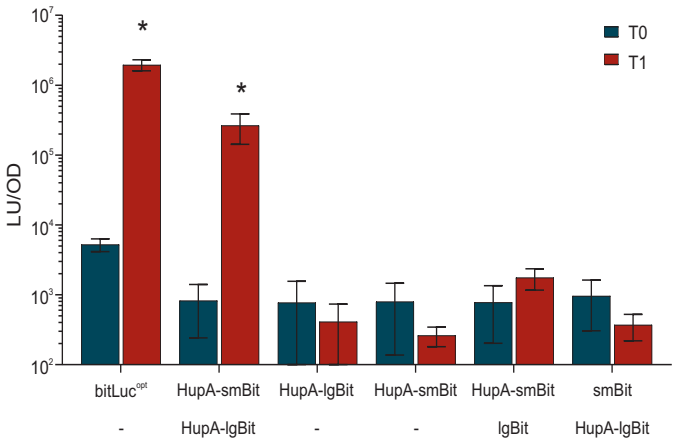
LU/OD
10^7
10^6
10^5
10^4
10^3
10^2
*
*
T0
T1
bitLuc^{opt}
HupA-smBit
HupA-lgBit
HupA-smBit
HupA-smBit
smBit
-
HupA-lgBit
-
-
lgBit
HupA-lgBit

Figure 4

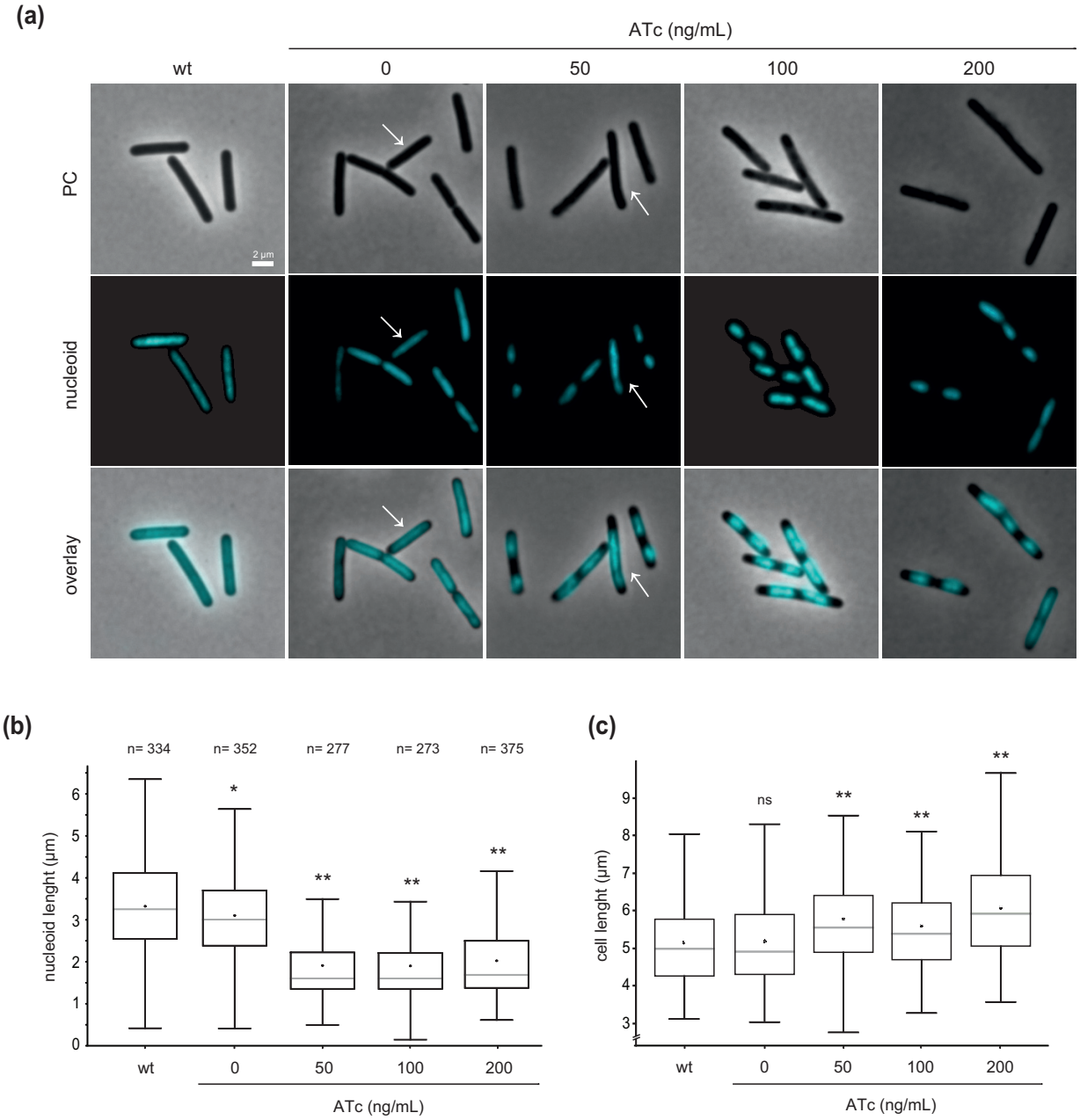
(a)
ATc (ng/mL)
wt
0
50
100
200
PC
nucleoid
overlay
2 µm
(b)
n= 334
n= 352
n= 277
n= 273
n= 375
nucleoid lenght (µm)
ATc (ng/mL)
(c)
ns
cell lenght (µm)
ATc (ng/mL)

Figure 5

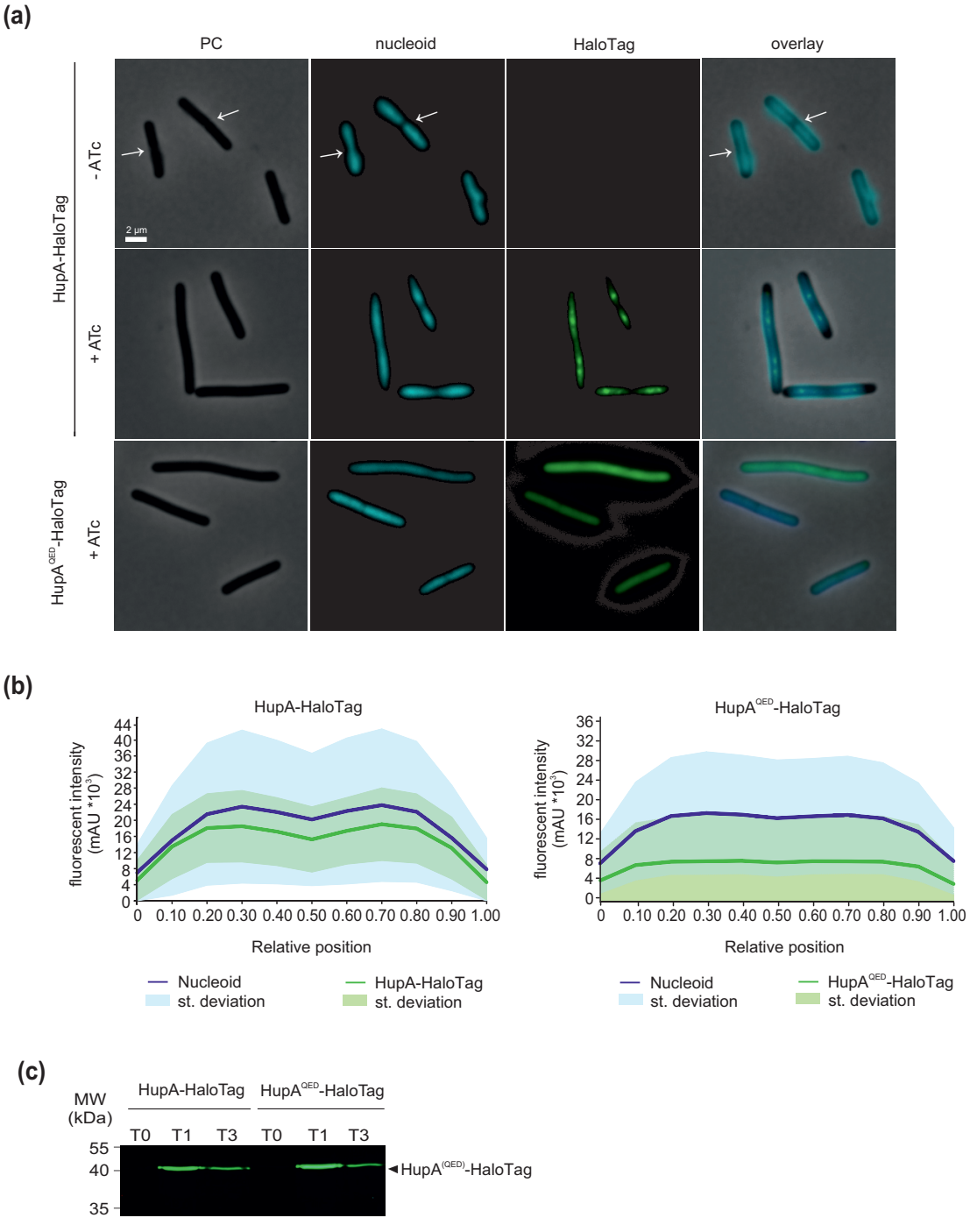
(a)
PC
nucleoid
HaloTag
overlay
HupA-HaloTag
- ATc
+ ATc
2 µm
HupA^QED-HaloTag
+ ATc
(b)
HupA-HaloTag
fluorescent intensity (mAU *10^3)
Relative position
Nucleoid st. deviation
HupA-HaloTag st. deviation
HupA^QED-HaloTag
fluorescent intensity (mAU *10^3)
Relative position
Nucleoid st. deviation
HupA^QED-HaloTag st. deviation
(c)
MW (kDa)
HupA-HaloTag
HupA^QED-HaloTag
T0 T1 T3 T0 T1 T3
55
40
35
HupA^(QED)-HaloTag

Figure 6

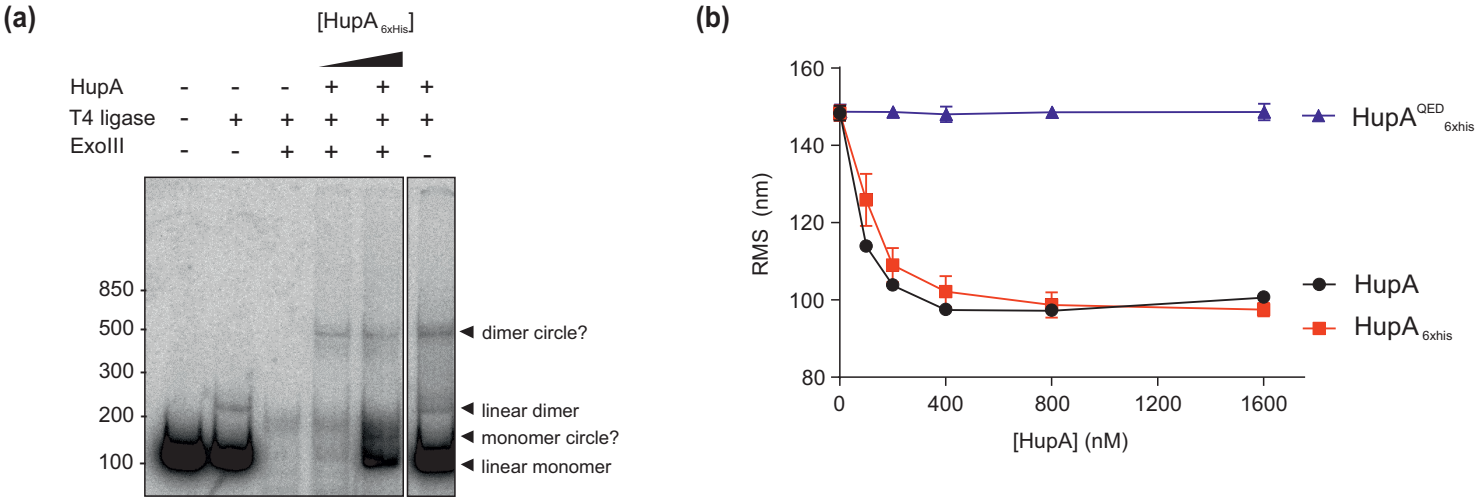
(a)
[HupA 6xHis]
HupA - - - + + +
T4 ligase - + + + + +
ExoIII - - + + + -
850
500
300
200
100
dimer circle?
linear dimer
monomer circle?
linear monomer
(b)
160
140
120
100
80
RMS (nm)
0
400
800
1200
1600
[HupA] (nM)
HupA QED 6xhis
HupA
HupA 6xhis

Figure 7

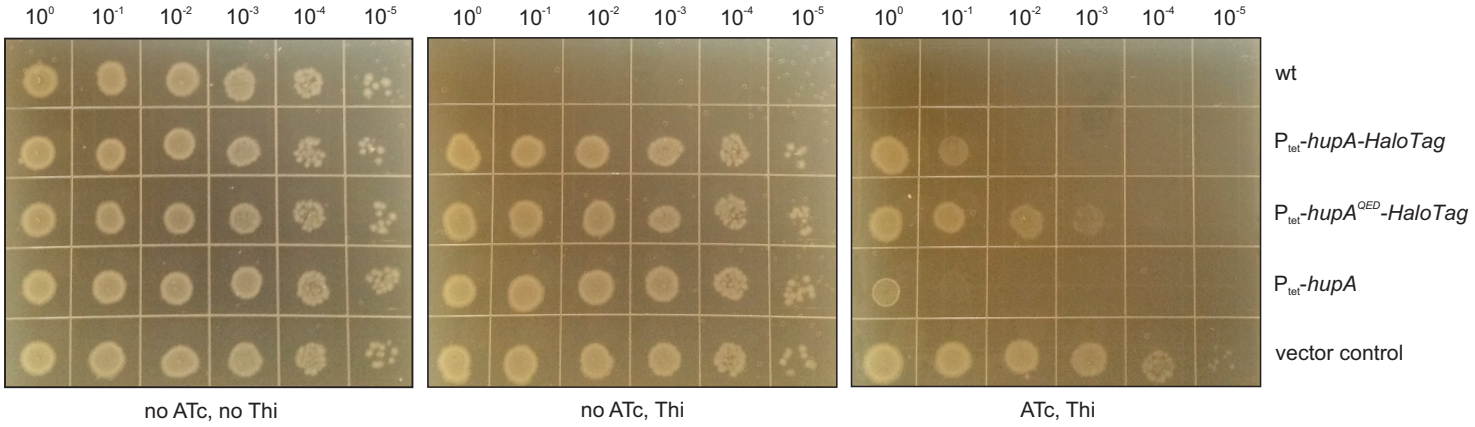
10^0 10^{-1} 10^{-2} 10^{-3} 10^{-4} 10^{-5}
wt
P_{tet}-*hupA-HaloTag*
P_{tet}-*hupA*^{QED}-*HaloTag*
P_{tet}-*hupA*
vector control
no ATc, no Thi
no ATc, Thi
ATc, Thi